In situ detection of tropospheric OH, HO_2, NO_2, and NO by laser-induced fluorescence in detection chambers at reduced pressures

Final Report for NASA grant NAG-1-1057

Principal Investigator: William H. Brune

For the period: 1 October, 1989 to 31 March, 1993

Department of Meteorology
Pennsylvania State University
University Park, PA 16802

24 June, 1992

Introduction

This final report is the summary of work completed for the grant entitled "In situ detection of tropospheric OH, HO_2, NO_2, and NO in detection chambers at low pressures". This work was supported by NASA under grant NAG-1-1057 and NSF under grant ATM-8909155 for the periods 1 October, 1989 to 31 March, 1993 and 15 April, 1990 to 14 September, 1993 respectively.

For detection of OH and HO2, we have met or exceeded most of the goals of the proposal for this grant. We have succeeded in building a prototype instrument for the detection of OH and HO_2 that has a detection sensitivity of about 2×10^4 (OH molecules cm^{-3})/(ct s^{-1}), about five times greater than proposed. The current minimum detectable OH of 1.4×10^5 OH molecules cm^{-3} (S/N=2; 30 second integration) is less than half that proposed, and will be much lower once scattered light levels are reduced.

The instrument displays other important properties. First, interfering signals from other gases and OH losses on the inlet appear to be small under laboratory and field conditions. Second, three different calibration methods, two external to the inlet, give similar results, to within 30%. Third, the chemical conversion efficiency of HO_2 to OH by addition of reagent NO is better than 90%. All of these factors give us great confidence that this technique works.

The instrument has gone through several variations that have not affected its potential performance but have affected its use. We were able to undergo the first field trials away from State College in June 1992, when we were able to participate informally in the ROSE experiment in rural Alabama, a year ahead of the proposed schedule for field studies. Because this field experiment was our first and the data analysis was complicated by instrument instabilities, we have not yet released the observations. None-the-less, we have gained insight into instrument design.

We have not yet completed all of the proposed work. The calibration systems need to be improved to reduce the 50% to 100% uncertainties to less than 30%. Interference signals from ambient gases and possible losses on the inlet under field conditions need to be quantified. Finally, the detection of NO_2 and NO with laser induced fluorescence is only now being seriously pursued. We have confidence that all of these projects will be completed by Fall, 1994.

In this final report we discuss several issues related to this work. We discuss in some detail the operation of the instrument, the test and calibration techniques and results, the comparison between the actual and proposed instrument, the observations from ROSE, and the development of the NO_2 instrument.

Appendix A is a preprint of a manuscript that we are submitting to the *Journal of Geophysical Research.* This report will summarize the work we have done. Technical details and figures can be found in the manuscript in Appendix A.

Instrument Design and Operation

The technique that we are using to detect OH and HO2 has been summarized in earlier reports. We repeat some of that discussion for this report.

The OH molecule is both excited and detected in the $A^2\Sigma(v'=0) \rightarrow X^2\Pi(v''=0)$ transitions near 308 nm, as opposed to exciting to the $A^2\Sigma(v'=1)$ state at 282 nm. Excitation at 308 nm produces substantially less laser-generated OH and organic molecule background fluorescence than excitation at 282 nm. At present, we tune the laser into resonance with the $Q_1(3)$ transition at 308.24 nm, but we can use other transitions as well.

To separate the prompt scattering (Rayleigh and chamber scattering) from the OH fluorescence, we pull the ambient air into a detection chamber through an inlet, and maintaining the pressure of the cell at $\sim$0.003 atm. With the quenching of the OH excited state reduced, the lifetime of the fluorescence extends beyond the laser pulse duration, and OH fluorescence can be detected after prompt scattering has ceased (called temporal filtering).

The instrument consists of a copper vapor laser-pumped dye laser that is frequency doubled into the ultraviolet and is multipassed through an evacuated detection chamber; a fast, gated detector with fast collection optics; a vacuum pump; and data collection electronics. The beam of ultraviolet laser light is focused into a White cell that has 24 passes The ultraviolet laser power is monitored at the exit of the White cell. This laser beam, with a repetition rate of 10 kHz, crosses the air stream in the center of the detection cell. At right angles to both the laser beam and the air flow is an optical train with fast, f#1 optics that focus the fluorescence onto a Hamamatsu microchannel plate detector, which has an 18 mm photocathode. The gain of the detector is normally reduced a factor of several thousand by a potential on a grid between the photocathode and the microchannel

plates, but is turned on for 300 nanoseconds approximately 30 nanoseconds after each laser pulse has cleared the White cell.

The ambient air is introduced into the detection cell through a 0.9 mm diameter hole, and the cell pressure is maintained at 3.5 Torr – 3.0 Torr from the atmosphere through the inlet, and 0.5 Torr from dry nitrogen or argon gas that is added at the White cell mirrors. The volumetric flow through the detection cell is 35 liters sec^{-1}. Nitrogen or argon gas is added to protect the White cell mirrors and to fill the volume of the detection chamber, thus confining the atmospheric air to a relatively narrow stream ($\sim 1.7 \pm .5$ cm dia.) in the middle of the detection chamber. A loop inside the detection chamber, located 7-20 cm upstream of the detection axis, is used to add either NO for conversion of HO_2 to OH or C_3F_6 for removal of OH as a test of the background signal.

Instrument Characterization

For an instrument based on the design of Hard and O'Brien, seven concerns must be addressed: sensitivity, calibration, minimum detectable OH, specificity, freedom from interference, OH/HO_2 inlet transmission, and detection of other species. The current status of our instrument for each one of these concerns will be briefly discussed here.

The governing equation for instrument sensitivity

The detected signal from fluorescence is a product of the excitation rate, the fluorescence collection efficiency, the fraction of excited state molecules that radiate and are not quenched, the density change of the airstream in the detection system, and the hydroxyl concentration. The equation The equation governing the sensitivity to OH is:

$$S_{OH} = \{B_{12}^{\rho}\frac{1}{c^2}(\frac{4ln2}{\Pi})^{1/2}(\Delta\nu_D^2 + \Delta\nu_l^2)^{-1/2}\frac{\Delta N}{N}P \cdot l\}\{\epsilon \cdot \eta \cdot T \cdot f_{gate}\}Q \cdot \frac{\rho_{in}}{\rho_{amb}} \cdot [OH]$$

where

S_{OH} is the detector signal in counts per second;

B_{12} is the Einstein B-coefficients for absorption from Dimpfle and Kinsey (1979);

$\Delta\nu_D$ and $\Delta\nu_l$ are the OH Doppler and laser line widths respectively;

P is the laser power in watts;

$\Delta N/N$ is the fraction of OH molecules in the rotational level being excited;

ϵ is the collection efficiency of the optics;

T is the transmission of the optics;

η is the quantum yield of the detector;

l is the length of the laser beam that overlaps the air stream:

Q is the quenching of the OH excited state;

f_{gate} is the fraction of OH fluorescence collected;

ρ_{in}/ρ_{amb} is the ratio of air densities inside the detection chamber and outside the inlet;

and $[OH]$ is the ambient concentration of OH outside the inlet.

Calibration

We have calibrated the detection sensitivity of the instrument using one internal and two external techniques. These three agree within experimental uncertainty with the calculated sensitivity of the detection axis, which is determined by measuring or estimating the value for each term in the equation that governs instrument sensitivity. The calculated values for the instrument sensitivity as a function of the detection cell density, and the observed, calibrated values are given in Figure 6 of Appendix A.

For the internal calibration, a low-pressure, discharge-flow tube was attached directly to the detection cell. Excess H atoms, produced in a microwave discharge or on a hot filament, were reacted with a known quantity of NO_2 to produce a known amount of OH. In September, 1991, the calibrated detection sensitivity, C, (given by the expression: $signal = C \times [OH]$) was $2.4 \pm 1.2 \times 10^{-6}$ (cts sec^{-1})/(OH molecule cm^{-3}), with the assumption that the inlet transmission of OH was 100%. For measurements in March, 1992, the calibrated detection sensitivity was $1.4 \pm 0.6 \times 10^{-5}$ (cts sec^{-1})/(OH molecule cm^{-3}). These sensitivities are obtained with average laser power of 15 mW, for which saturation of the OH transition is less than 20% (see Figure 4 of the Appendix). We have since increased the detection sensitivity another factor of three by replacing the interference filter in front of the detector.

The external calibration tests the sensitivity of the entire instrument. Two methods were used. First, a known amount of OH was produced by photolyzing a known amount of water vapor with a known flux of 185 nm radiation from a mercury lamp in a known amount of time. The absolute UV flux was determined with a photomultiplier tube that had been calibrated against a NIST secondary standard photodiode at the Calibration Test Facility at the Department of Physics at Johns Hopkins University. OH concentrations in the range of 10^7 to 10^9 cm^{-3} were produced in this technique.

Second, the absolute OH concentration was determined by absorption of a few percent of a laser beam that was passed 40 times over a 40 cm path just above the instrument inlet. The uncertainty of this technique is limited only by the uncertainties in the absorption cross sections and the uncertainties in the absorption measurements. Because we can measure only absorptions larger than a percent at present, due to laser instabilities, the amount of OH used in the calibration was in the range of 10^{11} to 10^{13} cm^{-3}, considerably above ambient levels.

These external calibration techniques indicate that the instrument sensitivity was 1.5×10^{-5} (ct s^{-1})/(OH molecule cm^{-3}) for March, 1992. The internal and external calibrations for March, 1992 agree to within 30%. The current instrument detection sensitivity is $(3.5 \pm 2.3) \times 10^{-5}$ cts sec^{-1}/ molecule cm^{-3}, for 15 mW average laser power and 2% water vapor in air. Thus, each count per second is equivalent to less than 3×10^4 OH molecules cm^{-3}, or less than 0.001 pptv at the ground.

Minimum detectable OH

The minimum detectable OH is dictated by the background signal. For our analysis thus far, the background signal is proportional to laser power, with the exception of ~1 ct sec^{-1} that is due to detector noise and 1-3 cts sec^{-1} that is due to solar scatter. We believe that this background is due to the "ringing" of the detection chamber with Rayleigh and chamber scattering. In September, 1991, this background signal was 10-15 cts sec^{-1}; in March, 1992, it was 20-40 cts sec^{-1}, depending on the exact alignment the input beam into the White cell on a given day. At present, the background signal is about 90 counts sec^{-1}, but will be reduced substantially with more careful baffle design.

As a result, the minimum detectable OH, given by

$$[OH]_{min} = \frac{S/N \cdot \sqrt{2 \cdot S_{bkgnd}}}{C \cdot \sqrt{time}}$$

for S/N = 2 and 15 mW average laser power is currently 1.4×10^5 molecules cm^{-3} (.004 pptv) for 30 seconds integration time, and is 4×10^4 molecules cm^{-3} for 5 minutes. Careful baffling should reduce the background signal a factor of 5, resulting in a factor of 2.2 lowering of the minimum detectable OH. This minimum detectable OH is adequate for OH and HO_2 measurements throughout the troposphere in a wide variety of conditions.

Specificity

One of the advantages of a spectroscopic technique is that the spectrum is a unique fingerprint of the molecule. Both the wavenumbers and the intensities of the observed fluorescence spectrum give us information. The spectrum of OH, shown in Figure 5 of Appendix A, comes from measurements of ambient HO_2 taken in September, 1991. This HO_2 was converted to OH by reaction with reagent NO, and the conversion efficiency for this measurement was considerably less than 100%, perhaps as low as only 5%. The $Q_1(3)$, $Q_{21}(3)$, and $P_1(1)$ lines are all evident, although the ratios are not correct because the ambient HO_2 abundance changed during the 2 minute spectral scan. We anticipate that with the improved instrument sensitivity we will obtain similar spectra for ambient OH in the summertime.

Freedom from interferences

One of the serious concerns with this technique has been the laser generation of OH within the detection cell itself. We have measured this laser-generated OH with our current detection system. We used rather extreme conditions to test for this interference signal: both 300 ppbv of ozone and 3% of water vapor were added to a flow of dry air in the laboratory. The resulting OH signal was 2 ± 2 cts sec^{-1}. The laser power for this experiment was 0.025 watts, which is about 1.5- 2.5 times larger than we will use during measurements. Thus, laser generated hydroxyl is not an issue with this instrument.

We are measuring the interference signal from other gases. Atmospheric abundances of hydrogen peroxide produce negligible signals. As discussed below, the background

signal is the same for measurements in the atmosphere as it is in the laboratory. This constancy indicates that non-resonant fluorescence from organic molecules or aerosols does not contribute significantly to the background signal for the environments tested.

OH and HO_2 inlet transmission

We have only begun to understand the inlet transmission of OH and HO_2 in our system. We can assume that any hydroxyl radical that hits a surface of our instrument is chemically destroyed. Thus, it is our goal to design and operate a "wall-less" detection system. We can have broken the problem of the inlet design into three areas: external surfaces, the throat, and internal surfaces. We have begun to investigate the use of suction through holes in the outer surface of the inlet to control the boundary layer.

Internally, the air flow is a jet expansion, and because we add a small flow of argon to the detection chamber, the air flow is kept contained and away from wall surfaces. From Schlieren studies, we know that the expanding air jet goes through an elliptically shaped shock front that extends 1 to 2 cm past the inlet. A secondary density gradient expands as a cone from this shock region, and the air velocity drops as the cross sectional area of the air stream increases. We continue to work on optimizing the inlet diameter and the distance between the inlet and the detection axis. Any small recirculation that is occurring just inside the inlet can be controlled by the proper addition of an inert gas.

We are left with the problem of the possible losses in the inlet throat itself, which can be tested by the combination of internal and external calibrations. However, the velocity in the instrument throat is roughly 300 m s^{-1}, and the possible contact time is only 10 μsec with the 3 mm thick inlet. A substantial transverse velocity, presumably generated by turbulence, of $>$ 100 m sec^{-1} is required to mix much of the air to the throat surface in this period of time.

Because the internal and external calibrations agree to within 30%, it appears that if any OH is lost on the inlet, it is less than half for laboratory conditions. In addition, different inlet designs (flat plates, cones) with different coatings (bare aluminum, Teflon and Halocarbon wax coatings) gave the same OH signal for a fixed source to within $\pm$20%. Thus, it appears that OH loss on the inlet is small. However, we will continue to investigate this important issue.

One concern about the jet expansion through the inlet is that the air stream gets cold for a short period before it goes through the shock front. Adducts may form at such low temperatures, and these possibilities need to be understood. Particular attention must be paid to the $HO_2 \cdot H_2O$ adduct, which is thought to affect the disproportionation reaction of HO_2.

We have tested this possibility as we examine the conversion efficiency for the HO_2 to OH conversion, as will be discussed below. We do this test by converting external OH to HO_2 with the external addition of CO, allowing it to flow through the inlet, and converting it back to OH with reagent NO. This test indicates that the losses for HO_2 and OH are the same for a range of water vapor amounts. Thus, adduct formation, at least with water vapor, does not appear to be occurring.

Detection of HO_2

The last concern is the detection of the hydroperoxyl radical, HO_2, by chemical conversion to OH by reaction with reagent NO, followed by LIF detection of the resulting OH. One of the difficulties in our high velocity system is that the mixing of reagent into the air stream and the chemical conversion of HO_2 to OH must occur in the same few milliseconds. This process can be accomplished by careful design of the NO injection system. Our current tests of changing the reaction time and the NO injector geometry show that we are getting excellent conversion efficiency of more than 90%).

We have two tests that indicate that the conversion of HO_2 to OH is better than (93±5)% complete if the inlet losses for OH and HO_2 are comparable. First, when water vapor is photolyzed, it produces OH and H atoms, which quickly react with any O_2 in the system to produce HO_2 in equal amounts to OH. When we clean the carrier gas of CO and hydrocarbons, we see $[OH] = [HO_2]$. Second, when OH is made with photolysis of water vapor, and CO is added to the airstream before it enters the instrument inlet, the OH reacts with the CO to form H, which then forms HO_2. The observed OH signal decreases. When NO is added inside the detection chamber, the OH signal produced from the conversion of HO_2 to OH equals the signal before CO was added to within 10%. This second test in particular indicates that the chemical conversion efficiency of HO_2 to OH is close to 1.

The high velocity and low air density in our system heavily favor the detection of HO_2, without the detection of RO_2 (see Figure 8 in Appendix A). Model simulations show that RO_2 is rapidly converted to RO by reagent NO, but that the reaction between RO and O_2 to produce HO_2 is much slower. From chemical model calculations, the RO_2 interference is below 6% when $[HO_2]= 0.5\times [RO_2]$ for a reaction time of 2 msec. We intend to devise tests for RO_2 sensitivity during the next three years.

Detection of Tropospheric OH and HO_2

We detected ambient OH during March, 1992, from the roof of the Walker Building, which houses our laboratory here at Penn State. The proportionality constant for the sensitivity was 1.5×10^{-5} (cts sec^{-1})/(OH cm^{-3}). With this system, we observed the signals for OH and HO_2 that are shown in Figure 12. The solid line is the signal in counts per second from the detection of the ambient air; the dotted line is from the resonance OH cell. The large signals are due to the addition of NO, and thus represent the HO_2 abundances. The conditions of the day were overcast skies, temperatures of about 35°C, and ozone and water vapor as shown.

The addition of hexafluoropropylene, denoted as C_3F_6, removes OH and produces a background signal that is essentially identical to the off-resonance background.

If we assume that the inlet transmission of OH is 95%, and we use the external calibration, adjusted for quenching in air, we find that on 18 March, 1992, in relatively clean air, that the ambient levels of OH in mid-afternoon were roughly $1 - 3 \times 10^6$ molecules cm^{-3} (see Figure 13 in Appendix A). The 1σ statistical uncertainty of each data point is $\pm 1 \times 10^5$ OH molecules cm^{-3}, giving a signal-to-noise ratio of 12; however, the absolute calibration is uncertain to about a factor of 2. Values of OH as low as 2×10^5 cm^{-3} were observed on this day.

The hydroperoxyl radical was also measured occasionally by the addition of reagent NO to the air stream inside the nozzle. The mixing of NO into the air stream for the instrument configuration at that time was not well known. However, if we assume a conversion efficiency of 95%, then the HO_2 abundances were approximately $6 - 9 \times 10^7$ cm^{-3}, or 2 to 3 pptv. The absolute accuracy of these numbers is probably a factor of two to three. The signal-to-noise ratio for HO_2 was 36 for 1 second.

Observations from ROSE II

In June, 1992, we were invited to participate informally in the Rural Ozone of the Southern Environment II experiment, which took place near Jachin, Alabama. These measurements were made in a rural pine forest in southwestern Alabama, and were a severe test of our instrument system at its early stage of development.

Because the tree canopy was at about 8 meters, we decided to place our detection system at 6 meters above the ground while keeping the lasers in a tent on the ground. This height gave us a better chance to obtain measurements that would be meaningful for the science. This new configuration was different from what we had used previously (see Figure 1 of Appendix A). Because the laser was so far away from the detection cell and its optics, instabilities caused mainly by thermal variations made measurements and their analysis difficult. This instability was complicated by our inability to control the temperature in the tent, and as a result, the laser power decreased a factor of ten over the course of the week of measurements. As a final result of these problems, both the detection sensitivity and the minimum detectable OH were degraded from the laboratory system.

Some interesting observations were obtained however. First, the HO_2 was observed to have concentrations less than 10 pptv, a factor of 5 to 10 less than predicted from photochemical models, the photostationary state of NO and NO_2, and the RO_2 chemical amplifier measurements from ROSE I. Second, OH was not unambiguously observed, and from the current analyses, had concentrations of less than 1×10^6 cm^{-3} at all times. This value is at least a factor of three less than predictions. In all of our tests since last year, we have not yet uncovered any problems with our instrument. However, more work needs to be done before we can be sure that our instrument was behaving properly and can publish our results.

A third interesting observation is that the large amounts of hydrocarbons in the forest did not increase the background signal (off-resonance) over the signal observed in the laboratory. Thus, this instrument appears to be insensitive to hydrocarbon fluorescence. Fourth, a signal due to HO_2, or perhaps to RO_2, persists several hours after sunset. Only a calibration of the instrument for sensitivity to RO_2 will enable us to distinguish between the two possibilities.

Remaining Concerns and Future Directions

The FAGE technique, using the equipment and techniques that we and others are developing, appears to be able to measure the OH and HO_2 amounts throughout the troposphere. It is sensitive enough, apparently free from interferences, and technologically feasible for a wide variety of environments. Several research groups in the United States and Europe now either have instruments of this type or are developing them. We feel that in a short time, most of questions about this technique will be resolved.

Chief among these issues is the potential for inlet losses of OH and HO_2. Such losses are the prime suspects for the low values of OH and HO_2 that we observed during ROSE II. We believe that if any OH loss is uncovered, it can be corrected by the proper manipulation of the flow.

Another issue is the calibration of the instrument. The techniques that are being used by us and others involve water vapor in nitrogen, with only a trace of oxygen. Techniques must be developed that add a known amount of OH to ambient air in an understandable way. The external calibration with absorption is capable of such measurements if the observable absorption can be decreased to the 10^{-4} range, so that OH concentrations of 10^9 cm^{-3} can be used.

A third issue involves the packaging of the instrument so that it can be used in a variety of environments and at the appropriate distances above the surface. The placement of the OH/HO_2 instrument is rapidly becoming as important as the measurement capability of the instrument itself. We feel that the advances in laser technology, coupled with careful design that emphasizes smaller, lighter instruments, will make OH/ HO_2 detection much more accessible in the future.

Finally, the work on developing a laser induced fluorescence system for the detection of NO_2 and NO really began only within the last year of the grant. The hardware for this system is just now being assembled, and will undergo the first tests by the end of the year. This technique is worth developing, even though the chemiluminescence technique is now well established, because of its immense potential. Although this technique at present requires an expensive laser system to be more sensitive than chemiluminescence, within a few years, diode lasers with enough energy near 585 nm will become available. Once small commercial diode lasers are available at a low cost, this technique will replace

chemiluminenscence for NO_2 monitoring and research. We would like to be part of the early development of this potentially important new technique.

List of Presentations and Publications

1. William H. Brune, Philip S. Stevens, and James H. Mather, "In situ detection of tropospheric OH and HO_2 by laser-induced fluorescence in a detection chamber at low pressure", invited presentation, Workshop on Local Measurement of Tropospheric HO_x, 23-26 March, 1992, SRI International, Menlo Park, CA.

2. P. S. Stevens, J. H. Mather, and W. H. Brune, "In-situ measurements of tropospheric OH and HO_2 by laser-indiced fluorescence at low pressures", contributed presentation, XXth Informal Conference on Photochemistry, 26 April -1 May, 1992, Atlanta, Georgia.

3. W. H. Brune, P. S. Stevens, and J. H. Mather, "Aircraft Instrument Design for In Situ Tropospheric OH Measurements by Laser-Induced Fluorescence at Low Pressure", invited presentation, International Symposium on Environmental Sensing, 22-26 June 1992, Berlin, Germany.

4. W. H. Brune, P. S. Stevens, and J. H. Mather, Measurements of tropospheric OH with laser-induced fluorescence", invited seminar, Summer Course on Diagnostic Tools in Atmospheric Physics, the International School of Physics "Enrico Fermi", 22 June - 2 July, 1993, Varenna, Italy.

5. P. S. Stevens, J. H. Mather, and W. H. Brune, "Measurement of Tropospheric OH and HO_2 by Laser-Induced Fluorescence at Low Pressure", submitted to *J. Geophys. Res.*, June ,1993.

Appendix A. A manuscript entitled "Measurement of Tropospheric OH and HO_2 by Laser-Induced Fluorescence at Low Pressure", submitted to the *Journal of Geophysical Research*

Measurement of Tropospheric OH and HO_2 by Laser-Induced Fluorescence at Low Pressure

P.S. Stevens, J.H. Mather and W.H. Brune

Department of Meteorology, The Pennsylvania State University,
University Park, Pennsylvania

Abstract

The hydroxyl radical (OH) is the primary oxidant in the atmosphere, responsible for many photochemical reactions that affect both regional air quality and global climate change. Because of its high reactivity, abundances of OH in the troposphere are less than 1 pptv, and thus difficult to measure accurately. This paper describes an instrument for the sensitive detection of OH in the troposphere using low-pressure laser-induced fluorescence. Ambient air is expanded into a low-pressure detection chamber, and OH is both excited and detected using the $A^2\Sigma^+(v' = 0) \rightarrow X^2\Pi(v'' = 0)$ transition near 308 nm. A loop injector upstream of the detection axis allows for the addition of reagent NO to convert ambient HO_2 to OH using the fast reaction $HO_2 + NO \rightarrow OH + NO_2$. Using recent advances in laser and detector technologies, this prototype instrument is able to detect less than 1×10^5 molecules cm^{-3} (0.005 pptv) of OH with an integration time of 30 seconds with negligible interferences.

Introduction

One of the most important species in tropospheric photochemistry and global climate change is the hydroxyl radical (OH). Reactions with OH are the primary loss mechanisms for a number of important species, such as methane and the alternative chlorofluorocarbons (HCFC's), which contribute to global warming and stratospheric ozone depletion. As a result, the lifetimes for these species are dependent on the OH concentration. In addition, OH initiates the oxidation of carbon monoxide and hydrocarbons, which in the presence of nitrogen oxides, produce ozone, peroxyacetylnitrate (PAN) and other pollutants. Because of this central role in atmospheric photochemistry, the hydroxyl radical is responsible for processes which occur on local, regional and global scales.

Despite the importance of OH in tropospheric photochemistry, very little is known about its abundance, and if it is changing over time. OH is formed in the troposphere from the photolysis of ozone and subsequent reaction of $O(^1D)$ with water vapor [*Logan et al.*, 1981; *Trainer et al.*, 1987]:

$$O_3 + h\nu\ (< 310nm) \rightarrow O(^1D) + O_2(^1\Delta_g) \tag{1}$$

$$O(^1D) + H_2O \rightarrow OH + OH \tag{2}$$

OH in the troposphere is primarily removed by reactions with carbon monoxide and methane,

$$OH + CO \rightarrow CO_2 + H \tag{3a}$$

$$H + O_2 + M \rightarrow HO_2 + M \tag{3b}$$

$$OH + CH_4 \rightarrow H_2O + CH_3 \tag{4a}$$

$$CH_3 + O_2 + M \rightarrow CH_3O_2 + M \tag{4b}$$

converting OH to the hydroperoxy radical (HO_2) and the methoxy radical (CH_3O_2). Similar to the reaction with methane, OH oxidizes many hydrocabons, forming other peroxy

radicals (RO_2). HO_2 and RO_2 are rapidly cycled back into OH through reactions with nitric oxide, ozone, and O_2, resulting in a photochemical equilibrium between OH and HO_2/RO_2:

$$HO_2 + NO \rightarrow OH + NO_2 \quad (5)$$

$$HO_2 + O_3 \rightarrow OH + 2O_2 \quad (6)$$

$$RO_2 + NO \rightarrow RO + NO_2 \quad (7)$$

$$RO + O_2 \rightarrow R'HO + HO_2 \quad (8)$$

Since the recognition of the important role the OH radical plays in tropospheric chemistry [*Weinstock et al.*, 1969; *Levy*, 1971; *Crutzen*, 1974], many attempts have been made to measure its abundance over the past 20 years. Because of the high reactivity of OH, predicted mixing ratios in the troposphere are extremely small (less than 1 pptv, $\sim 1 \times 10^7$ molecules cm^{-3}) [*Logan et al.*, 1981; *Perner et al.*, 1987]. These predictions are in reasonable agreement with empirically derived OH abundances determined from chemical lifetime measurements of methyl chloroform, a compound with well known anthropogenic sources [*Prinn et al.*, 1987]. Methyl chloroform is removed from the atmosphere by reaction with OH, and thus its lifetime is directly related to the OH abundance. However, because the lifetime of methyl chloroform in the atmosphere is long (6 years), OH concentrations derived in this manner reflect global average abundances. Although OH concentrations derived from this empirical method are extremely valuable, they have yet to be verified by direct measurements. In addition, uncertainties in source strengths and oceanic losses for methyl chloroform prevent a rigorous test of photochemical models.

The small mixing ratios of OH in the troposphere are extremely difficult to measure accurately, especially on the short time scale required as a test of the rapid photochemistry of OH. Early local measurement attempts were plagued by interferences and uncertainties [*Ortgies et al.*, 1980; *Davis et al.*, 1981 a,b], and as a result, theoretical models of tropo-

spheric OH have advanced far beyond the experimental measurements. However, a number of local measurement techniques have advanced to the point where reliable OH measurements are now being made, and are ready to provide a true test of photochemical theories. A recent intercomparison between two different OH measurement techniques resulted in measured OH concentrations substantially below model predictions [*Mount and Eisele*, 1992]. This discrepancy suggests that our knowledge of tropospheric photochemistry may be incomplete, thus limiting our ability to predict with confidence how changes in the composition of the atmosphere may affect global climate change in the future [*Thompson*, 1992].

Methods for detecting OH locally in the troposphere include both spectroscopic and non-spectroscopic approaches. Spectroscopic techniques include laser-induced fluorescence [*Bradshaw et al.*, 1984; *Hard et al.*, 1984, 1986; *Shirinzadeh et al.*, 1987; *Chan et al.*, 1990; *Hofzumahaus et al.*, 1990] and long-path absorption [*Dorn et al.*, 1988; *Armerding et al.*, 1990; *Hofzumahaus et al.*, 1991; *Mount*, 1992]. These techniques have the advantage of specificity, however in the past they have suffered from background interferences which limited the overall sensitivity of the instruments. Non-spectroscopic techniques rely on chemical conversion of OH to a species which is more easily detected, such as the ion-assisted method [*Eisele and Tanner*, 1991], and the radiocarbon CO method [*Felton et al.*, 1990]. Although highly sensitive, these techniques require careful analysis to prevent spurious OH production in the titration scheme. With the exception of long-path absorption, all OH measurement techniques require careful calibrations to account for interactions of the sampling process with ambient air.

Methods for detecting HO_2 also include both spectroscopic and non-spectroscopic approaches. Non-spectroscopic techniques include chemical conversion to OH [*Hard et al.*, 1992a], and chemical amplification of both HO_2 and RO_2 through a series of chain reactions followed by detection of NO_2 [*Cantrell et al.*, 1984; *Hastie et al.*, 1991]. Spectroscopic techniques include matrix isolation/ESR detection of HO_2 [*Mihelcic et al.*, 1990], as well

as infrared absorption [*Nelson and Zahniser*, 1991].

Laser-induced fluorescence (LIF) remains a promising technique for the detection of OH, offering both high sensitivity and selectivity. Although OH has been measured successfully in the stratosphere and lower mesosphere using fluorescence techniques [*Anderson*, 1976; *Stimpfle and Anderson*, 1988; *Stimpfle et al.*, 1989], applications of these techniques to tropospheric OH measurements has been difficult. Initial attempts utilized the $A^2\Sigma\ v' = 1 \leftarrow X^2\Pi\ v'' = 0$ electronic transition of OH at 282 nm, and observed the red-shifted fluorescence from the $A^2\Sigma\ v' = 0 \rightarrow X^2\Pi\ v'' = 0$ band near 308 nm [*Wang et al.*, 1976; *Davis et al.*, 1976]. The advantage of using this transition is that it easily allows the spectral isolation of the fluorescence from scattering of the laser pulse. Although this approach works well in the stratosphere, the high concentration of both water vapor and ozone in the troposphere results in the generation of OH by the laser itself through reactions (1) and (2), and broad-band fluorescence of other species excited by the 282 nm radiation added to the background signals [*Ortgies et al.*, 1980; *Davis et al.*, 1981 a, b]. These interferences proved to be quite severe, producing background OH signals which were often higher than ambient, reducing the overall sensitivity of these instruments.

A number of techniques have been introduced to reduce these interferences [*Wang et al.*, 1981]. One of the most notable of these is the sampling of ambient air at low pressure through an inlet. This technique was first developed by Hard *et al.* [1984] and called FAGE (Fluorescent Assay by Gas Expansion). Sampling ambient air at a low pressure reduces the concentration of interferring species, such as O_3 and H_2O, thus reducing the chemical reaction rates that produce OH from the laser pulse. The total signal resulting from OH fluorescence does not change appreciably because the reduction in OH concentration upon expansion is offset by the decreased collisional quenching rate at the lower pressure, which results in an increased quantum yield for fluorescence. The decreased collisional quenching rate at the low pressure also results in an increased lifetime of the OH excited state, which extends the fluorescence beyond the length of the laser pulse. Thus OH fluorescence, which

lasts a few hundred nanoseconds, can be discriminated by electronic gating from Rayleigh and Mie scattering, chamber scatter, and fluorescence from species such as SO_2 and CH_2O, which have shorter radiative lifetimes.

Although low-pressure sampling greatly reduced much of the interference previously encountered, early versions of the FAGE technique still suffered from high background signals due to laser-generated OH [*Hard et al.*, 1984, 1986; *Chan et al.*, 1990]. Performing the excitation at 282 nm with a low repetition-rate laser system, with high energy per pulse, resulted in interference signals which were higher than ambient levels by a factor of 23 [*Smith and Crosley*, 1990]. Although the contribution of this interference to the total signal was determined through chemical removal of ambient OH in the flow system, the presence of these high backgrounds presented a significant limitation to the sensitivity of the instrument.

By using a high repetition-rate laser, with low energy per pulse, the internally generated OH can be reduced without sacrificing overall sensitivity. With a high average power, a higher repetition-rate laser system maintains a high OH fluorescence signal. The disadvantage of using a high repetition-rate laser is that it requires a high flow velocity in the detection region to prevent exposure of the same air mass to multiple pulses of the laser beam, which could lead to OH generation.

The laser-generated OH interference can be further reduced by both exciting and detecting in the $A^2\Sigma\ v' = 0 \rightarrow X^2\Pi\ v'' = 0$ band near 308 nm. The photodissociation of O_3 at 308 nm is reduced a factor of 25, and the yield of $O(^1D)$ is reduced a factor of 5, when compared to excitation at 282 nm, in the production of OH (reactions 1 and 2) [*Hofzumahaus et al.*, 1990; *Hard et al.*, 1992b]. The disadvantage of this approach, as mentioned above, is the difficulty in isolating the OH fluorescence signal from scattered radiation.

Despite the difficulties mentioned above, the use of high repetition-rate laser systems, and excitation of OH at 309 nm and at low pressure has become a promising LIF technique

for the fast and specific detection of OH in the troposphere. The present version of FAGE [*Chan et al*, 1990], as well as a similar instrument under development by Hofzumahaus *et al.* [1990] are incorporating these approaches. This paper describes a LIF instrument, based on the FAGE technique, which is capable of measuring OH and HO_2 in the troposphere with insignificant interferences. Using recent advances in laser and detection technologies, this instrument is capable of detecting less than 1×10^5 OH molecules cm^{-3} (0.005 pptv) with a S/N = 2 in 30 seconds.

Instrument Description

The instrument consists of (1) a laser system to generate the excitation radiation, (2) the OH sampling chamber, (3) a fast, gated detector and collection optics. The prototype instrument, used to make ambient measurements on the roof of the Walker Building at the University Park campus of the Pennsylvania State University, is shown in Figure 1.

Laser System. A 15-W, air cooled copper-vapor laser (Oxford Lasers), operating at 10 kHz and equipped with an unstable resonator, pumps a grating-tuned dye laser (Lambda Physik FL-3001). The output of the dye laser is frequency doubled from the red at 616 nm into the UV using a KDP crystal. The dye solution consists of a mixture of Rhodamine 640 (0.15 gm/L, Exciton), and Kiton Red (0.4 gm/L, Exciton) in ethanol. This dye mixture maximizes production of 616.5 nm (red) radiation from both the 510 nm (green) and 578 nm (yellow) output of the copper-vapor laser. At peak operating conditions, approximately 50-mW of doubled UV (20-nsec pulse length, 0.15-cm^{-1} line width) is produced from approximately 1 W of 616 nm output from the dye laser and 12-15 W from the copper-vapor laser. Typical operating conditions were at lower UV power to prevent saturation of the OH transition. A glan-laser prism separates the vertically polarized undoubled red fundamental beam from the horizontally polarized UV beam.

Before exiting the dye laser, the UV beam passes through an evacuated cell where OH is generated through thermal dissociation of ambient H_2O. This cell provides a reso-

nance fluorescence OH signal as a reference to indicate when the dye laser is tuned into resonance with the OH transition. A 25-W alumel filament produces the reference OH, and the fluorescence is detected at approximately 1 torr using a Hamamatsu 760 photomultiplier tube located directly opposite of the filament. The detector is equipped with an interference filter and a UG-11 color-glass filter which isolates the fluorescence from the glowing filament.

Sampling Chamber. After exiting the dye laser, the UV beam is focussed into a White cell inside the sampling chamber. The optical layout is shown schematically in Figure 2. The beam crosses the air stream in 24 non-overlapping 2-mm by 5-mm beams at the center of the cell, separated along the direction of the flow by less than 10 mm. The UV laser power is monitored at the exit of the White cell.

Ambient air is introduced into the sampling chamber through a 0.93-mm diameter inlet centered on a flat plate. Pressure inside the chamber is maintained at 3.5 torr, with 0.5 torr from the addition of dry nitrogen or argon gas at the White cell mirrors. The volumetric flow rate inside the chamber is 35 liters sec^{-1}. The additional flow perpendicular to the flow, and along the axis of the White cell, serves to keep the White cell mirrors clean and to fill the detection volume, confining the ambient air stream to the center of the chamber. A loop injector, located directly below the inlet and 7-20 cm upstream of the detection axis is used for chemical addition. The inside of the chamber is coated with Teflon to reduce radical loss; however air that passes through the detection region does not contact these walls. A schematic of the internal flow is shown in Figure 3. The initial configuration of the instrument placed the inlet 11 cm above the detection axis (Figure 3a). The jet passed through a 5-cm diameter, 7.6-cm length flow tube before entering the nominally 7.6-cm diameter detection region, 3.8 cm above the laser beam path. The velocity of the jet at the detection axis in this configuration was 314 m sec^{-1}. Subsequently, the inlet and injector were raised an additional 10 cm with a 5-cm diameter flow tube insert to increase the reaction time for chemical conversion (Figure 3b). The velocity of the jet at the detection

axis was reduced to 70 m sec^{-1}. The velocity in this configuration is still greater than the 50 m sec^{-1} minimum velocity required to prevent exposure pf the same air mass to multiple pulses of the 10 kHz laser beam. A 124 cfm mechanical pump (Leybold #S160) provides the flow velocity.

HO_2 is detected by the addition of NO to the air stream to convert ambient HO_2 to OH using reaction (5) ($k_{298} = 8.6 \times 10^{-12}$ cm^3 $molecule^{-1}$ sec^{-1} [*DeMore et al.*, 1992]). NO (Matheson, CP grade) is added through the loop injector located directly below the inlet. The NO passes through an Ascarite trap before injection into the system. Typical flow rates of NO are 0.2 to 1 sccs.

Detector and collection optics. The OH fluorescence is collected at right angles to both the air flow and the laser beams through an f#1 optical train, and focussed onto a Hamamatsu micro-channel plate (MCP) detector (R2024U-06) (Figure 2). This detector has a 18-mm photocathode, recessed in the surrounding housing by 17 mm. To prevent vignetting, a 150-mm focal length diverging lens in front of the detector collimates the fluorescence onto the photocathode. The collimated fluorescence passes through a 25-mm UG-11 filter, which is 65% transmitting at 308 nm, and a 25-mm interference filter which is described in detail below.

The gain of the detector is normally reduced a factor of 9000 by a potential grid between the photocathode and the microchannel plate. The detector is turned on (rise time = .23 nsec) by applying a 12 V bias to the control grid approximately 30 nsec after each laser pulse has exited the White cell, and remains on for 300 nsec to collect the OH fluorescence. Thus, the OH fluorescence is isolated from Rayleigh and chamber scatter.

Although the current gain and quantum efficiency of the micro-channel plate (MCP) detector (5×10^5 and 5-6%) are both less than that for a photomultiplier tube (typically 2×10^6 and 20%), the loss of photon sensitivity is offset by the low background signals associated with the gating system of the MCP. A memory of the high Rayleigh scatter associated with the laser in a photomultiplier tube results in a high background signal

long after the pulse [*Chan et al.*, 1990; *Crosley*, 1992]. The ability to quickly turn on the MCP after the laser pulse without any associated memory or ringing increases the ultimate OH detection sensitivity of this system.

The output signal of the MCP is amplified by a 280 MHz preamplifier (Stanford Research Systems SR440) with an overall gain of 91. The amplified signal is then counted by a 200 MHz gated photon counter with a built-in discriminator (Stanford Research Systems SR400). The counter gate is opened 40-50 nsec after the laser pulse, 10-20 nsec after the detector gate.

Instrument Performance

Several concerns must be addressed in order to assess the performance of a LIF instrument based on the FAGE technique: sensitivity, selectivity, minimum detectable OH, calibration, including HO_2 conversion efficiency, and interferences, including laser generated OH and detection of other species.

Sensitivity and selectivity. The detection sensitivity, C, is given as the signal due to OH fluorescence divided by the OH concentration:

$$C = S_{\mathrm{OH}}/[\mathrm{OH}] \tag{9}$$

The detection sensitivity is dependent on the excitation rate, the collection efficiency of the optics and detector, the fraction of molecules in the excited state which radiate, and the density change upon expansion of air into the sampling chamber. The overall sensitivity of the instrument is also dependent on the transmission OH and HO_2 through the inlet. This issue will be treated separately below. The governing equation for the sensitivity is given by:

$$C = \left[\frac{B_{12}^{\rho}}{c^2}\left(\frac{4ln2}{\Pi}\right)^{1/2}\left(\Delta\nu_D^2 + \Delta\nu_l^2\right)^{-1/2}\frac{\Delta N}{N}\cdot P\cdot l\right]\left[\epsilon\cdot\eta\cdot T\cdot f_{\mathrm{gate}}\right]Q\cdot\frac{\rho_{\mathrm{in}}}{\rho_{\mathrm{amb}}} \tag{10}$$

S_{OH} detector signal in counts sec^{-1}.

B_{12}	Einstein B-coefficients for absorption [*Dimpfle and Kinsey*, 1979].
$\Delta\nu_D$ and $\Delta\nu_l$	OH Doppler and the laser line widths, respectively.
P	laser power in watts.
$\Delta N/N$	fraction of OH molecules in the rotational level being excited (calculated).
ϵ	collection efficiency of the optical train (calculated).
T	transmission of the optics (measured and estimated).
η	quantum yield of the detector (measured).
l	length of the laser beam overlapping the ambient air stream (calculated).
Q	quenching of the OH excited state [*German*, 1975; 1976; *Cleveland and Wiesenfeld*, 1988].
f_{gate}	fraction of the OH fluorescence collected (measured).
$\rho_{\text{in}}/\rho_{\text{amb}}$	ratio of air densities inside and outside the sampling chamber (measured).

A number of uncertainties are associated with the calculated sensitivity of the instrument, most notably the actual overlap of the laser beam with the ambient airstream, and the actual field of view of the detector. The values for these parameters for the instrument during various stages of development are listed in Table 1. The initial version of the prototype (9-91) suffered from a low "effective" quantum efficiency of the micro-channel plate due to electronic interference from the copper-vapor laser. Electronic discrimination against this interference caused a significant loss of the fluorescence pulses reaching the counter. Improved shielding of the pre-amplifier reduced this interference, allowing the use of lower discriminator levels. Additional improvements of the subsequent version of the prototype (3-92) included the addition of a mirror opposite the detection optics ($\times 1.7$) and antireflection coatings on all of the detection optics ($\times 1.5$). These versions employed a 25-mm, 8-nm-band-pass, $\sim$10% transmissive interference filter centered at 309 nm (Barr Associates). The latest version of the prototype (7-92) includes a 25-mm, 8-nm-band-pass, 35% transmissive interference filter (Barr Associates).

As can be seen from equation (10), the sensitivity of LIF based OH detection is proportional to laser power. However the effective laser power is limited by saturation

of the OH electronic transition, which occurs when the ground electronic state of OH becomes depleted due to absorption of the pump radiation. Once the electronic transition is saturated, the remaining photons per pulse from the pump laser do not yield any additional fluorescent signal. The detected fluorescence signal varies almost linearly with the average laser power in the White cell for a stable OH concentration, as shown in Figure 4.. The sensitivities in Table 1 are calculated based on an average laser power of 15 mW, and as shown Figure 4, saturation of the OH transition at this power is less than 20%.

Comparison of the ambient air spectrum with the reference cell spectrum of OH demonstrates the selectivity of the instrument. Figure 5 shows a spectrum of OH from partially converted ambient HO_2 after reagent NO addition, along with the reference OH spectrum. The $Q_1(3)$, $Q_{21}(3)$, and the $P_1(1)$ lines of OH are clearly shown in the ambient spectrum. The relative intensities of the lines reflect the change in ambient HO_2 over the time of the scan (2-3 minutes). This scan was taken with the 3-92 version of the prototype instrument. Similar spectra for ambient OH in the summertime should be possible with the improved sensitivity of the 7-92 version.

Minimum detectable OH. The sensitivity, C, and the background signal determine the minimum detectable OH, given by:

$$[\mathrm{OH}]_{min} = \frac{S/N\sqrt{2 \cdot S_{bkg}}}{C\sqrt{time}} \tag{11}$$

For version 9-91, the background signal was 10-15 cts sec^{-1} for a laser power of 15 mW, resulting in a calculated minimum detectable OH of 5×10^5 molecules cm^{-3} in nitrogen for a signal-to-noise ratio (S/N) of 2 and an averaging time of 30 sec. With an averaging time of 5 minutes, the minimum detectable OH is 1.6×10^5 molecules cm^{-3}. For version 3-92, the background was 30 cts sec^{-1} at 15 mW, resulting in a calculated value of 1×10^5 molecules cm^{-3} in 30 sec and 3.2×10^4 molecules cm^{-3} in 5 min and in nitrogen for $[\mathrm{OH}]_{min}$ ($S/N = 2$). Of this background signal, 1-3 cts sec^{-1} is due solar scatter, and approximately 1 ct sec^{-1} is due to detector noise. The remaining background signal is

proportional to laser power, and is probably due to "ringing" of Rayleigh and chamber scatter inside the sampling cell. At present, the background signal for the latest version is approximately 90 cts sec^{-1} at 15 mW, but careful baffling of the laser beam in the sampling chamber should reduce this signal by a factor of 2 to 5, giving an expected value for $[OH]_{min}$ of approximately 4×10^4 molecules cm^{-3} in 30 sec and 1.3×10^4 molecules cm^{-3} in 5 minutes ($S/N = 2$).

The dependence of the calculated sensitivity and minimum detectable OH concentration on the density of nitrogen inside the detection chamber is illustrated in Figure 6 for the prototype versions using 15 mW of laser power. The lifetime of the OH excited state (τ), the quenching of the fluorescence (Q), and the fraction of fluorescence collected by the fixed gate (f_{gate}), all have a strong dependence on the pressure inside the detection chamber. As mentioned above, these effects roughly cancel the decrease in OH concentration upon expansion into the cell at the low pressures ($\rho_{\mathrm{in}}/\rho_{\mathrm{amb}}$). As a result, the calculated sensitivity and the minimum detectable OH change by less than 30% for air densities between 0.002 and 0.01 atm (Figure 6d - 6e). Thus small changes in internal pressure have little effect on the overall sensitivity of the instrument. The sensitivity of the instrument in air is reduced by 30% due to quenching of the OH excited state by O_2. Changes in the water vapor content of the ambient air also affects the instrument sensitivity as much as 30% due to quenching of the excited state. Thus, measurements of ambient OH must be accompanied by measurements of ambient H_2O to determine the instrument calibration.

Calibration. The most important and difficult aspect of the low pressure LIF technique is the absolute calibration of the instrument. The difficulty lies in the problem of producing a known concentration of OH at atmospheric pressure. For the low-pressure LIF technique, the problem can separated into internal and external calibrations, with the ratio reflecting the transmission of OH through the sampling inlet. The internal calibration can be accomplished using well established discharge-flow techniques for the production of known quantities of OH at pressures less than 5 torr [*Howard*, 1979; *Brune et al.*, 1983].

For the external calibration, OH is produced at atmospheric pressure from the photolysis of water vapor in two different systems. The first system produces OH concentrations on the order of ambient levels, and are calculated from the rate of water vapor photolysis. The second system produces OH concentrations which are high enough to be measured by UV absorption directly above the inlet.

To calibrate the internal detection axis, a 2.5-cm I.D., 66-cm long flow tube is inserted into the sampling chamber, just above the detection axis. This configuration is a resonable representation of the airflow distribution from the nozzle at the detection axis (Figure 3). OH radicals in this system are produced by titrating known concentrations of NO_2 with an excess of H atoms using the fast $H + NO_2 \rightarrow OH + NO$ reaction ($k_{298} = 1.3 \times 10^{-10}$ cm^3 $molecule^{-1}$ sec^{-1}) [*DeMore et al.*, 1992]. H atoms are produced using a microwave discharge of trace H_2 in a flow of He using a phosphoric acid quartz tube, or thermal dissociation of trace H_2 in He on a tungsten filament. NO_2 is added to the system through a movable injector. The position of the NO_2 injector is adjusted to maximize the production of OH, and to minimize the loss of OH due to the $OH + NO \rightarrow HONO$ reaction.

The internal calibrations were performed in 2-3 torr of N_2. Air was not used because of complications in the titration scheme resulting from the reaction of H atoms with O_2 (reaction 3b). NO_2 concentrations were varied from less than 1×10^8 to 2×10^9 cm^{-3}, while H concentrations were maintained at approximately $1 - 2 \times 10^{11}$ cm^{-3}. Because of high background signals due to the production of OH impurity from the microwave discharge, average laser power for these calibrations were less than 1 mW. The uncertainty associated with these calibrations is $\pm 30\%$.

The external calibration of the instrument employed two different techniques. The first technique involves the production OH from the photolysis of a known amount of water vapor with a known flux of 185 nm radiation from a mercury lamp in a known amount of time:

$$H_2O + h\nu(< 246nm) \rightarrow OH + H \qquad (12)$$

OH concentrations are produced in the external flow system according to the photolysis equation

$$[OH] = [H_2O] \cdot \sigma_{H_2O} \cdot F_{185} \cdot \Delta t \quad (13)$$

where $[H_2O]$ is the water vapor concentration in the flow system, measured using a chilled mirror hygrometer (General Eastern), σ_{H_2O} is the absorption cross section of water vapor at 185 nm (5.5×10^{-20} cm^2) [*DeMore et al.*, 1992], F_{185} is the photon flux at 185 nm, and Δt is the photolysis exposure time (0.2-0.3 sec).

A 20-cm long, 7.5-cm I.D. flow tube is placed above the inlet to the LIF sampling chamber. Approximately 500 STD cm^3 sec^{-1} of N_2 is bubbled through distilled H_2O before entering the flow tube. Nitrogen, from liquid boil-off, was used instead of air to reduce the amount of reactive impurities in the system. The fraction of flow not captured by the inlet is vented through a screen below the nozzle. To produce a laminar airflow, the gas passes through a cluster of 8 100 × 100-mesh wire cloth and a set of 3-mm-I.D., 25-mm long flow straighteners. The photolysis source, located 2-5 cm above the inlet, consists of an 2.5-cm Hg lamp (Oriel) positioned end-on outside the flow tube. UV radiation is passed through a 25-mm diameter, 100-mm-f.l. lens and baffled by 25-cm by 3-cm rectangular mask, creating sheet of radiation across the airflow. The UV flux at 185 nm is measured using either a Hamamatsu R1187 phototube, or an absolutely calibrated EMR 541G photomultiplier tube. The EMR tube was calibrated at the Calibration Test Facility in the Physics Department at Johns Hopkins University against a photodiode that was recently calibrated at NIST. OH concentrations between 1×10^7 and 2×10^8 moleules cm^{-3} were produced in this system and were varied by changing the water vapor fraction in the main N_2 flow. Laser power for these calibrations were between 1 to 15 mW. To insure that the OH production was due solely to 185 nm photolysis of H_2O, a ~20% bandpass filter, centered at 186 nm (Acton Research) was placed in front of the UV source for some calibrations.

A crucial aspect of this calibration technique is the removal of reactive impurities

from the system in order to insure that the OH concentration calculated from equation (13) does not change significantly before entering the LIF detection region. Purified N_2, from liquid boil-off, was passed through approximately 500 gm of dried Hopcalite (Callery) to reduce impurity CO to less than 1 ppbv. To insure that reactive loss of OH was minimal, the distance between the photolysis source and the inlet was varied, resulting in OH concentration changes of less than 15%. The purity of the system was also monitored by measuring the HO_2 concentration produced by the photolysis source. Photolysis of water vapor from reaction (12) produces one H atom for every OH molecule. The H atoms are converted to HO_2 through reaction (3b) in the prescence of trace O_2 in the system. In the absence of impurities which convert OH to HO_2, such as CO and hydrocarbons, this photolytic source produces equivalent concentrations of OH and HO_2. Assuming the absense of chemical loss during calibrations when $[OH]=[HO_2]$, the uncertainty associated with the calculated OH concentrations at the present time is not less than 50%. This reflects the uncertainty associated with the radial distribution of the both the gas velocity in the source and the UV flux crossing the airstream.

The second external calibration technique eliminates the problem of reactive impurities in the system by measuring the absolute concentration of OH using absorption of UV radiation just above the inlet to the LIF sampling chamber. The disadvantage of this technique is that the small cross section of OH requires concentrations over 1000 times greater than ambient levels in order to measure the absorption over a short path length. However, this absorption external calibration technique together with the above photolysis technique establishes the linearity of the instrument sensitivity over a wide dynamic range.

A 30.5-cm long, 10-cm wide absorption cell, 25-cm high, is placed above the inlet to the LIF sampling chamber. A set of 8 100 × 100-mesh wire cloth and a set of ~3-cm diameter, 5-cm long hexcell flow straighteners establish a laminar profile of a > 1 STD liter sec^{-1} flow of N_2 and H_2O, purified as before. Nitrogen was used instead of air so that these external calibrations could be directly compared to the results of the photolysis

calibration technique. Two 12.7-cm long Hg lamps (BHK), placed end-to-end along the length of the absorption cell, provide a uniform field of UV radiation 5-cm above the inlet to the sampling chamber. A small fraction of the UV laser radiation is diverted before entering the LIF detection chamber, and is directed into a White cell located directly above the inlet. The beam crosses the length of the absorption cell 40 times, resulting in an effective path length of 1000 cm. The UV beam is detected at the exit of the White cell using a photodiode.

Absolute OH concentrations are determined from the intensity of the UV beam using Beer's law

$$[\mathrm{OH}] = \ln\left(\frac{I_o}{I}\right) \cdot \sigma^{-1} \cdot L^{-1} \cdot \left(\frac{n_j}{n_o}\right)^{-1} \tag{14}$$

where I_o/I is the ratio of the reference intensity of the laser to the absorbed intensity using the $Q_1(3)$ OH line, σ is the integrated absorption cross section for OH (2.4×10^{-15} cm^2), L is the effective path length in cm, and n_j/n_o is the fraction of OH molecules in the rotational level where the absorption transition originates (0.075 for the $Q_1(3)$ branch at 298 K). OH concentrations as high as 1×10^{12} cm^{-3} were produced in this system.

To insure the uniformity of the OH concentration profile along the absorption axis, the entire cell was moved along the axis relative to the inlet, resulting in OH concentration variations of less than 10%. The OH concentration was varied over a limited range ($\sim$ $2 \times 10^{11} - 1 \times 10^{12}$ cm^{-3}) by changing the water vapor fraction in the main N_2 flow. Detection of OH concentrations less than 2×10^{11} cm^{-3} was limited by laser noise. The total laser power entering the LIF detection cell was reduced to less than 0.005 mW to maintain reasonable signal levels at these high OH concentrations. The photodiode was linear with laser power from 0.005 mW to 3 mW as determined by inserting neutral density filters into the beam. At these low laser powers and high OH concentrations, non-linearity of the MCP detector was approximately 20%. The uncertainty associated with this absorption calibration at the present time is not less than 50%, reflecting the uncertainty associated with the measurement of the laser power and the measured absorption signal.

Results of the calibrations of the prototype versions are summarized in Table 2. Internal calibrations were performed on the earliest versions of the prototype, while external calibrations were performed with the latest two versions. The values for the external calibrations incorporate both the photolysis and the absorption techniques. These are illustrated in Figure 7 for the 7-92 version. Calibrations based on the two different external calibration techniques agree to within 50%. The sensitivities and minimum detectable OH in nitrogen for these versions using 15mW of laser power are compared to the calculated sensitivities in Figure 6e. The $\sim$ 45% difference between the external and internal calibrations for the 3-92 version is mainly due to the different quenching environments for each calibration. The external calibrations reflect the sensitivity of the system under high concentrations of water vapor ($\sim$ 2%) and thus are in better agreement with the calculated sensitivities for nitrogen with 2% water vapor. The internal calibrations are performed under dry conditions. As can be seen from Figure 6e and Table 2, the expected and calibrated sensitivities agree to within 40%.

Based on the relative agreement between the internal and external calibrations (accounting for the different quenching environments) the reactive loss of OH on the inlet is less than 20%. for this system. This is not surprising given the rapid velocity of the airstream at the throat of the nozzle. Different inlet designs (flat and conical) and surfaces (bare aluminum, Teflon and Halocarbon wax coatings) gave the same OH signal to within 20%. This insensitivity of the instrument's performance to the shape of the nozzle as well as the coating of the external surfaces imply that loss is not occuring near the throat of the inlet. However, given the large uncertainty presently associated with the external calibrations, small losses of OH on the inlet are difficult to quantify.

The instrument sensitivity was monitored in the field by continuous measurements of laser power at the exit of the White cell. The laser power is the most likely term in equation (10) to exhibit large fluctuations in the field, but certainly not the only variable that may change. Presently, the instrument sensitivity is also monitored in the field by

periodic measurements of Rayleigh scatter, made by allowing the detection cell to fill with the dry N_2 or Ar confining flow. The ratio of OH detection sensitivity and Rayleigh and Raman scattering detection sensitivity is given by:

$$\frac{C_{OH}}{C_R} \sim \frac{\sigma_0}{\sigma_{Ray}} \left(\frac{4 \ln 2}{\pi}\right)^{1/2} \cdot (\Delta\nu_L^2 + \Delta\nu_D^2)^{-1/2} \cdot \left(\frac{\Delta N}{N}\right) \cdot Q \cdot \frac{f_{gate}}{f_{pol}} \qquad (15)$$

σ_0 and σ_{Ray}	scattering cross sections by OH and air.
$\Delta\nu_D$ and $\Delta\nu_l$	OH Doppler and the laser line widths, repectively.
$\Delta N/N$	fraction of OH molecules in the rotational level being excited.
Q	quenching of the OH excited state.
f_{gate}	fraction of the OH fluorescence collected.
f_{pol}	fraction of the polarized Rayleigh scattering measured.

Variations in the optical geometry, collection efficiency and laser power which affect the OH detection sensitivity is reflected by changes in the observed Rayleigh scatter signal. For a given temperature and pressure, $\Delta N/N$ is fixed and Q can be calculated and verified through measurements. The stability of f_{gate} and $\Delta\nu_L$ can also be determined. Thus sensitivity of the instrument to scattering, combined with laboratory measurements of the relationship of scattering to OH sensitivity, reflects the absolute calibration of the instrument.

The conversion efficiency of HO_2 to OH was determined using a simple titration technique employing the photolytic OH calibration system described above. OH produced in the source is first converted externally to HO_2 by adding a small flow of a 12 ppm mixture of CO in N_2 (Matheson) ([CO] $\sim 1 \times 10^{13}$ cm^{-3}). This converts the external OH to HO_2 through reactions (3a) and (3b). The HO_2 is then converted back to OH inside the chamber through NO addition through the loop injector. Assuming that any losses upon expansion into the sampling chamber are similar for both OH and HO_2, changes in the total HO_x signal (OH + HO_2) due to external CO addition simply reflects the conversion efficiency of HO_2 to OH. This simple experiment eliminates a number of uncertainties

associated with other HO_2 calibration methods involving the measurement of the decay of HO_2 due to self reaction in an external reactor [*Hard et al.*, 1992a]. The efficiency of the 9-91 version was only 7% due to insufficient reaction time, and poor mixing of the NO with the internal airstream. For the 3-92 and the 7-92 versions of the prototype, this efficiency was improved to 93±5% by increasing the overall reaction time with NO, and by decreasing the size of the loop injector, allowing for more efficient mixing with the airstream. This efficiency is comparable to kinetic simulations of the system, which indicate a conversion efficiency of greater than 95%.

The OH signal produced from addition of NO to the ambient airstream is due to HO_2 rather than RO_2, as computer simulations of the kinetics indicate (Figure 8). RO_2 is converted to HO_2 in the presence of NO and O_2 through reactions (7) and (8). Although the conversion of RO_2 to RO by NO is rapid in this system, the short reaction time and low air density prevents the rapid conversion of RO to HO_2. As shown in Figure 8, when $[RO_2]=[HO_2]$, less than 2% of the observed converted OH signal is due to ambient RO_2. More quantitative tests are still required to verify this interference.

Interferences. As mentioned above, laser-generated OH has been the most serious interference of previous LIF techniques to measure tropospheric OH. This interference is substantially reduced in the present system due to the laser excitation technique and the low pressure sampling of ambient air. To test the system for the production of OH by the laser, 300 ppbv of ozone and 3% water vapor were added to a flow of air in the laboratory. Under these extreme conditions, the resulting OH signal was only 2±2 counts sec^{-1} ($\sim 10^5$ OH cm^{-3}) with a laser power of 25 mW at 308 nm using version 3-92 of the prototype. This laser power is almost a factor of 2 greater than the maximum laser power used in field measurements. Thus, interferences due to laser-generated OH is insignificant in this system.

The other significant interference mentioned above is the broad-band fluorescence of other species excited by the laser radiation. Atmospheric abundances of hydrogen peroxide

produced in the laboratory does not produce a significant background signal in this instrument (< 2 counts sec−1)). Potential interfences from other molecules, such as SO_2 and CH_2O will be tested as part of future calibration measurements. As discussed below, the background signal measured in the atmosphere is the same as it is in the laboratory using dry N_2 as the source gas. This implies that broad-band fluorescence of organic molecules or aerosols does not contribute significantly to the instrument background signal.

Results and Discussion

The early versions of the prototype were used to measure ambient OH and HO_2 from the roof of the Walker building on the Penn State campus. Figure 9 shows the signal levels for OH and HO_2 taken on September 17, 1991 with the 9-91 version of the prototype instrument. In this figure, the solid line is the observed signal in counts sec^{-1} from ambient air, while the dotted line is the OH signal from the reference cell, indicating when the dye laser is tuned into resonance with the $Q_1(3)$ transition at 308.24 nm. The larger signals in the figure are the result of NO addition to the ambient airstream and thus represent HO_2 abundances. Data is collected every second, and is displayed as 10-sec averages in the top panel, and 30-sec averages in the second panel to improve the signal-to-noise level.

The vertical scale has been expanded in the second panel of Figure 9 to emphasize the signal due to ambient OH. The on-resonance signal due to ambient OH of ~10 counts sec^{-1} is clearly seen above the off-resonance background signal of ~ 16 counts sec^{-1}. This background is primarily due to laser scattering in the detection cell, as indicated from the correlation of the variation of the laser power in the bottom panel with the off-resonance signal. The magnitide of the background signal was independent of the ambient conditions and was identical to background signals measured in the laboratory. There are two cases in Figure 9, at 3:35-3:37 and 3:51-3:53, where the OH signal decreases even though the laser remained tuned on resonance with the OH transition. In these cases, denoted by "C_3F_6" in the figure, perfluoropropylene (CF_3CFCF_2, Matheson, 99.5%) was added through the loop

injector to remove ambient OH from the airstream through the fast OH + C_3F_6 → adduct reaction ($k_{298} = 2 \times 10^{-12}$ cm^3 molecule^{-1} sec^{-1} [P. Wennberg, unpublished data, 1991; *McIlroy and Tully*, 1993]. This "chemical modulation" of the OH signal serves as a test for the contribution of laser-generated OH to the observed signal. OH produced in the path of the White cell does not have sufficient time to react with C_3F_6 before detection, and a signal due to this interference would remain above the off-resonance background signal. Perfluoropropylene is used as the chemical modulator because it does not contain hydrogen atoms which, in addition to H_2O, could serve as a source of laser-generated OH. Because the chemical and spectral backgrounds in Figure 9 are the same, interference due to laser-generated OH is small, and the observed signal is due solely to ambient OH.

Figure 10 shows a 30-minute segment of data taken on September 17, 1991. The top panel shows the ambient and reference cell signals averaged over 10 seconds. The on-resonance signal of ~5-6 counts sec^{-1} can still be seen above the off-resonance background signal even though the laser power during this segment was 33% lower than that for Figure 9. The second panel in this figure shows both the UV solar flux (filled circles, measured using a silicon photodiode equipped with a UG-11 visible filter) as well as the total solar flux (open circles). Small variations in the OH signal correlate well with variations in the solar UV flux and O_3 around 12:20-12:22. The gradual drop of the on-resonance signal after 12:24 corresponds to the drop in the solar UV, which remains low as the total solar flux changes due to variations in the cloud cover. The small increase in the OH signal after 12:34 correlate with the small rise in the O_3 concentration, even though the solar UV flux does not appear to change significantly. The correlation of the observed OH signal with variations in photochemical sources for OH suggest that variations in the observed signal are not due to instrument artifacts.

Assuming that loss of ambient OH on the inlet is small (based on the 3-92 internal and external calibrations) the instrument sensitivity constant, C, was $(2.4 \pm 1.2) \times 10^{-6}$ (counts sec^{-1})/(molecule cm^{-3}) using the 9-91 internal calibration adjusted to account

for the increased quenching of the OH excited state in air. Figure 11 shows the diurnal trend for OH and HO_2 for Septermber 17, 1991. As can be seen from this figure, midday levels of OH were were highly variable due to cloudy conditions, with a slow decline under clear skies in the afternoon, under relatively clean conditions. Ozone mixing ratios averaged about 60 ppbv, and water vapor was 1600 ppmv. The 1σ statistical uncertainty in these measurements of OH and HO_2 is about 30% of the peak values, while the absolute uncertainty is about 50% due to the uncertainty associated with the absolute calibrations mentioned above.

Periodic measurements of HO_2 by the addition of NO are also shown in Figure 11. Because of poor mixing and the limited reaction time for the 9-91 version, the conversion efficiency for these measurements was only about 7%. Because of this low conversion efficiency, the uncertainty in the HO_2 concentrations is larger for these measurements than that for the OH measurements. The conversion efficiency was improved to 93% by reducing the loop diameter of the injector, thus increasing the mixing of NO with the ambient airstream. In addition, the reaction time was increased by increasing the distance between the loop injector and the detection axis. With these improvements, HO_2 can now be detected with the same uncertainty as for OH.

Measurements were made with the improved 3-92 version on March 18, 1992 on the roof of the Walker building under cloudy, winter conditions. Ozone mixing ratios were approximately 35 ppbv, and water vapor was 3000 ppmv. The laser power for these measurements was less than optimum, averaging about 7-8 mW over the course of the day. Based on the internal and external calibrations for this version, the instrument sensitivity constant on this day was $(7.3 \pm 0.5) \times 10^{-6}$ (counts sec^{-1})/(molecule cm^{-3}), adjusted to account for the increased quenching of the OH fluorescence in air. The improved sensitivity of the instrument is shown in Figure 12, where the signal due to ambient OH and HO_2 is displayed as 4-sec averages. Addition of C_3F_6, as shown in the figure, resulted in chemical background signals which agreed well with the off-resonance background. The signal-to-

noise ratio for OH was 12 in 30 seconds, and 36 in 1 second for HO_2.

Figure 13 shows the OH and HO_2 data for the March 18, 1992 measurements. The frequency of data is not representive of the capability of the instrument, as measurements were interrupted to allow for configuation tests of the flow and HO_2 conversion efficiency. Early morning concentrations of OH were only $3 - 4 \times 10^5$ molecules cm^{-3}, near the detection limit of the instrument. A frontal passage in the afternoon coincided with a sudden rise in OH and HO_2. During this episode, cloud cover decreased the total solar flux by a factor of 2, ozone increased by 5 ppbv, and water vapor varied from 1500 ppmv to 3000 ppmv. OH concentrations peaked at $(2.2 \pm 1.0) \times 10^6$ molecules cm^{-3} in the afternoon, before falling off to less than 7×10^5 molecules cm^{-3}, 2-3 hours after the frontal passage. HO_2 abundances were approximately $(6 \pm 1) \times 10^7$ molecules cm^{-3} during this episode. Clearly there were not enough measurements of other important species to estimate the expected OH concentration during this episode, but the rough correlation of OH with O_3 and H_2O suggests that the sudden rise in OH concentration was due to the passage of an airmass in a different photochemical equilibrium over the instrument.

Conclusions

Although previous attempts to measure tropospheric OH by laser-induced fluorescence have suffered from uncertainties associated with a number of interferences generated by the technique itself, the prototype instrument described above has been designed to minimize these interferences. Specifically, exciting and detecting OH in the $A^2\Sigma^+ v' = 0 \rightarrow X^2\Pi v'' = 0$ band near 308 nm using a high repetition-rate laser system reduces interference from laser-generated OH to negligible levels, as well as eliminating broad-band fluorescence from other ambient species. The incorporation of a fast-switching micro-channel plate detector allows temporal gating of the Rayleigh scatter associated with the laser pulse, which avoids the high noise levels associated with transient saturation of photomultiplier tubes. HO_2 can be detected with the same sensitivity as OH by the addition of NO to the ambient

airflow. Because of the reduction in pressure, conversion of ambient RO_2 to OH resulting from NO addition is small.

This instrument has the advantages of both sensitivity and selectivity in the measurement of tropospheric OH and HO_2. Although it is clear that sensitive measurements of ambient OH and HO_2 can be made with this instrument, the absolute calibration of this instrument still requires some improvement, and additional potential interferences need to be investigated. The largest uncertainty associated with the present instrument is in the absolute calibration of the inlet transmission of OH and HO_2. Although the present calibrations indicate insignficant losses of OH and HO_2 on the inlet, they still require some improvement in order to decrease the present uncertainty of ~50%. In addition to inlet loss, the effect of adduct formation in the cooled jet expansion needs to be addressed, specifically the $HO_2 \cdot H_2O$ complex, which may affect the disproportionation of HO_2 and OH. The effect of adduct formation involving HO_2 in this instrument seems unlikely given the high calibrated conversion efficiency of HO_2 to OH. Also, the effect of the instrument sensitivity with varying ambient conditions, such as different trace gas concentrations, wind speed and direction across the nozzle and temperature needs to be studied in further detail as part of future calibration measurements.

Future improvements to the calibration techniques will include a redesigned UV source for the photolytic calibration which will increase the production of OH, remove the uncertainty associated with the flux distribution, and allow variations in the total flux, thus producing variable OH concentrations under constant concentrations of water vapor. External calibrations will then be performed under both "wet" and "dry" conditions, allowing more direct comparisons to internal calibrations under similar quenching conditions. Reduction of the power fluctuations associated with the UV laser beam should allow the absorption technique to measure OH concentrations down to less than 10^{11} cm^{-3}. These improvements should reduce the uncertainty in both techniques to less than 20%, and effectively increase the precision of the overall calibration by overlapping the OH concen-

tration range covered by each method. External calibrations will also be performed in air rather than nitrogen, resulting in a more accurate calibration of the instrument under ambient quenching conditions. Various trace gases, such as SO_2 and CH_2O, will be added to the external flow to determine any potential fluorescent interference with the detection of ambient OH. Also, the effect of air motion across the nozzle on the transmission of OH through the inlet will be examined during field measurements by studying possible correlations of the detected OH signal with wind speed and direction. These tests and improvements should further quantify the various potential effects of inlet sampling and ambient interferences on the instrument sensitivity.

The minimum detectable OH and HO_2 for this instrument of less than 1×10^5 molecules cm^{-3} in 30 seconds is sufficient for measurement throughout the troposphere. In conjunction with measurements of CO, NO_x, water vapor, ozone and other species, the fast measurements of OH and HO_2 by this instrument is capable of providing a true test of photochemical models of the troposphere.

Acknowledgements. We would like to thank C. Fong for experimental assistance, Russ Pelton for calibration of our photomultiplier tube, and P. Wennberg, A. Hofzumahaus, F. Eisele and G. Mount for many helpful discussions. This work was supported by the National Science Foundation (grant ATM-8909155) and NASA (grant NAG-1-1057).

References

Anderson, J. G., The absolute concentration of OH ($X^2\Pi$) in the earth's stratosphere, *Geophys. Res. Lett., 3*, 165, 1976.

Armerding, W., A. Herbert, M. Spiekermann, J. Walter, and F. J. Comes, Fast scanning laser DOAS - A very promising technique for monitoring OH and other tropospheric trace gases, *Fresenius J. Anal. Chem., 340*, 654, 1991.

Bradshaw, J. D., M. O. Rogers, and D. D. Davis, Sequential two-photon laser-induced

fluorescence: A new technique for detecting hydroxyl radicals, *Appl. Opt., 23*, 2134, 1984.

Brune, W. H., J. J. Schwab, and J. G. Anderson, Laser magnetic resonance, resonance fluorescence, and resonance absorption of the reaction kinetics of $O + OH \rightarrow H + O_2$, $O + HO_2 \rightarrow OH + O_2$, $N + OH \rightarrow H + NO$, and $N + HO_2 \rightarrow$ products at 300 K between 1 and 5 torr, *J. Phys. Chem., 87*, 4503, 1983.

Cantrell, C. A., D. H. Stedman, and G. J. Wendel, Measurement of atmospheric peroxy radicals by chemical amplification, *Anal. Chem., 56*, 1496, 1984.

Chan, C. Y., T. M. Hard, A. A. Mehrabzadeh, L. A. George, and R. J. O'Brien, Third-generation FAGE instrument for tropospheric hydroxyl measurement, *J. Geophys. Res., 90*, 18,569, 1990.

Cleveland, C. B., and J. R. Wiesenfeld, Electronic quenching of highly rotationally excited OH ($A^2\Sigma^+$, v'= 0, 1) by H_2O, *Chem. Phys. Lett., 144*, 479, 1988.

Crosley, D. R., Local measurement of tropospheric HO_x, *NASA Conf. Publ.*, to be published, 1993.

Crutzen, P., A discussion of the chemistry of some minor constituents in the stratosphere and the troposphere, *Pure Appl. Geophys., 106*, 1385, 1973.

Crutzen, P., Photochemical reactions initiated by and influencing ozone in unpolluted tropospheric air, *Tellus, 26*, 47, 1974.

Davis, D. D., W. Heaps, and T. McGee, Direct measurements of natural tropospheric levels of OH via an aircraft borne tunable dye laser, *Geophys. Res. Lett., 3*, 331, 1976.

Davis, D. D., M. O. Rogers, S. D. Fischer, and K. Asai, An experimental assessment of the O_3/H_2O interference problem in the detection of natural levels of OH via laser induced fluorescence, *Geophys. Res. Lett., 8*, 69, 1981a.

Davis, D. D., M. O. Rogers, S. D. Fischer, and W. S. Heaps, A theoretical assessment of the O_3/H_2O interference problem in the detection of natural levels of OH via laser induced fluorescence, *Geophys. Res. Lett., 8*, 73, 1981b.

DeMore, W. B., S. P. Sander, D. M. Golden, R. F. Hampson, M. J. Kurylo, C.

J. Howard, A. R. Ravishankara, C. E. Kolb, and M. J. Molina, Chemical kinetics and photochemical data for use in stratospheric modeling, *JPL Publ. 92-20*, 1992.

Dimpfle, W. L., and J. L. Kinsey, Radiative lifetimes of OH ($A^2\Sigma$) and Einstein coefficients for the A-X system of OH and OD, *J. Quant. Radiat. Transfer, 24*, 233, 1979.

Dorn, H. P., J. Callies, U. Platt, and D. H. Ehhalt, Measurement of tropospheric OH concentrations by laser long-path absorption spectroscopy, *Tellus, 40(B)*, 437, 1988.

Eisele, F. L., and D. J. Tanner, Ion-assisted tropospheric OH measurements, *J. Geophys. Res., 96*, 9295, 1991.

Felton, C. C., J. C. Sheppard, and M. J. Campbell, The radiochemical hydroxyl radical measurement method, *Environ. Sci. Technol., 24*, 1841, 1987.

German, K. R., Radiative and predissociative lifetimes of the v'= 0, 1 and 2 levels of the $A^2\Sigma^+$ state of OH and OD, *J. Chem. Phys., 63*, 5252, 1975.

German, K. R., Collision and quenching cross sections in the $A^2\Sigma^+$ state of OH and OD, *J. Chem. Phys., 64*, 4065, 1976.

Hard, T. M., R. J. O'Brien, C. Y. Chan, and A. A. Mehrabzadeh, Tropospheric free radical determination by FAGE, *Environ. Sci. Technol., 18*, 768, 1984.

Hard, T. M., C. Y. Chan, A. A. Mehrabzadeh, W. H. Pan, and R. J. O'Brien, Diurnal cycle of tropospheric OH, *Nature, 322*, 617, 1986.

Hard, T. M., C. Y. Chan, A. A. Mehrabzadeh, and R. J. O'Brian, Diurnal HO_2 cycles at clean air and urban sites in the troposphere, *J. Geophys. Res., 97*, 9785, 1992a.

Hard, T. M., A. A. Mehrabzadeh, C. Y. Chan, and R. J. O'Brien, FAGE measurements of tropospheric HO with measurements and model of interferences, *J. Geophys. Res., 97*, 9795, 1992b.

Hastie, D. R., M. Weissenmayer, J. P. Burrows, and G. W. Harris, Calibrated chemical amplification for atmospheric RO_x measurements, *Anal. Chem., 63*, 2048, 1991.

Hofzumahaus, A., H.-P. Dorn, and U. Platt, Tropospheric OH radical measurement techniques: recent developments, in *Physico-chemical behavior of atmospheric pollutants*,

edited by G. Restelli and G. Angeletti, pp. 103-108, Kluver, 1990.

Hofzumahaus, A., H.-P. Dorn, J. Callies, U. Platt, and D. H. Ehhalt, Tropospheric OH concentration measurements by laser long-path absorption spectroscopy, *Atmos. Environ., 25A*, 2017, 1991.

Howard, C. J., Kinetic measurements using flow tubes, *J. Phys. Chem., 83*, 3, 1979.

Levy, H., Normal atmosphere: Large radical and formaldehyde concentrations predicted, *Science, 173*, 141, 1971.

Logan, J. A., M. J. Prather, S. C. Wofsy, and M. B. McElroy, Tropospheric chemistry: A global perspective, *J. Geophys. Res., 86*, 7210, 1981.

McIlroy, A., and F. P. Tully, Kinetic study of OH reactions with perfluoropropene and perfluorobenzene, *J. Phys. Chem., 97*, 610, 1993.

Mihelcic, D., A. Volz-Thomas, H. W. Pätz, D. Kley, and M. Mihelcic, Numerical analysis of ESR spectra from atmospheric samples, *J. Atmos. Chem., 11*, 271, 1990.

Mount, G. H., The measurement of tropospheric OH by long path absorption 1. Instrumentation, *J. Geophys. Res., 97*, 2427, 1992.

Mount, G. H., and F. L. Eisele, An intercomparison of tropospheric OH measurements at Fritz Peak Obeservatory, Colorodo, *Science, 256*, 1187, 1992.

Nelson, D. D., and M. S. Zahniser, Diode laser spectroscopy of ν_3 vibration of HO_2, *J. Mol. Spec., 150*, 527, 1991.

Ortgies, G., K.-H. Gericke, and F. J. Comes, Is uv laser induced fluorescence a method to monitor tropospheric OH? *Geophys. Res. Lett., 7*, 905, 1980.

Perner, D., U. Platt, M. Trainer, G. Hübler, J. W. Drummond, D. H. Ehhalt, G. Helas, W. Junkermann, R. Rudolph, B. Schubert, K. J. Rumpel, and A. J. Voltz, Tropospheric OH concentrations: A comparison of field data with model predictions, *J. Atmos. Chem., 5*, 185, 1987.

Prinn, R., D. Cunnold, R. Rasmussen, P. Simmonds, F. Alyea, A. Crawford, P. Fraser, and R. Rosen, Atmospheric trends in methylchloroform and the global average for the

hydroxyl radical, *Science, 238*, 945, 1987.

Shirinzadeh, B., C. C. Wang, and D. Q. Deng, Diurnal variation of the OH concentration in ambient air, *Geophys. Res. Lett., 14*, 123, 1987.

Smith, G., and D. R. Crosley, A photochemical model of ozone interference effects in laser detection of tropospheric OH, *J. Geophys. Res., 95*, 16427, 1990.

Stimpfle, R. M., and J. G. Anderson, In-situ detection of OH in the lower stratosphere with a balloon borne high repetition rate laser system, *Geophys. Res. Lett., 15*, 1503, 1988.

Stimpfle, R. M., L. B. Lapson, P. O. Wennberg, and J. G. Anderson, Balloon borne in-situ detection of OH in the stratosphere from 37 to 23 km, *Geophys. Res. Lett., 16*, 1433, 1989.

Thompson, A. M., The oxidizing capacity of the earth's atmosphere: Probable past and future changes, *Science, 256*, 1157, 1992.

Trainer, M., E. Y. Hsie, S. A. McKeen, R. Tallamraju, D. D. Parrish, F. C. Fehsenfeld, and S. C. Liu, Impact of natural hydrocarbons on hydroxyl and peroxyl radicals at a remote site, *J. Geophys. Res., 92*, 11879, 1987.

Wang, C. C., L. I. Davis, C. H. Wu, and S. Japar, Laser-induced dissociation of ozone and resonance fluorescence of OH in ambient air, *Appl. Phys. Lett., 28*, 14, 1976.

Wang, C. C., L. I. Davis, P. M. Selzer, and R. Munoz, Improved airborne measurements of OH in the atmosphere using the technique of laser-induced fluorescence, *J. Geophys. Res., 86(C)*, 1181, 1981.

Weinstock, B., Carbon Monoxide: Residence time in the atmosphere, *Science, 166*, 224, 1969.

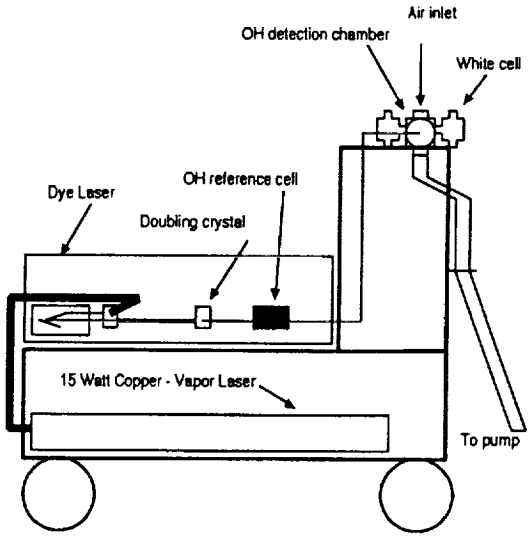

Figure 1. Schematic of the prototype OH/HO_2 instrument.

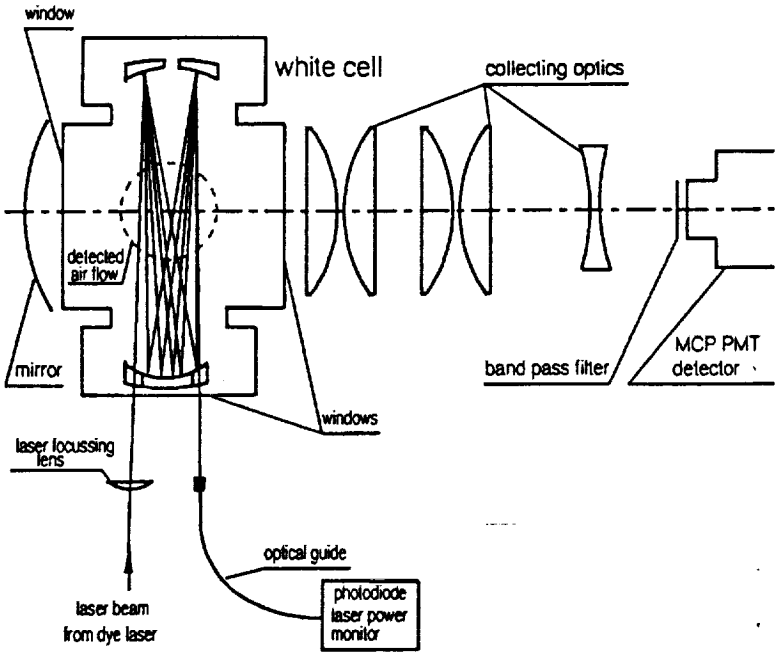

Figure 2. Optical layout of the OH/HO_2 instrument, including the White cell and the collecting optics leading to the microchannel plate detector (MCP PMT).

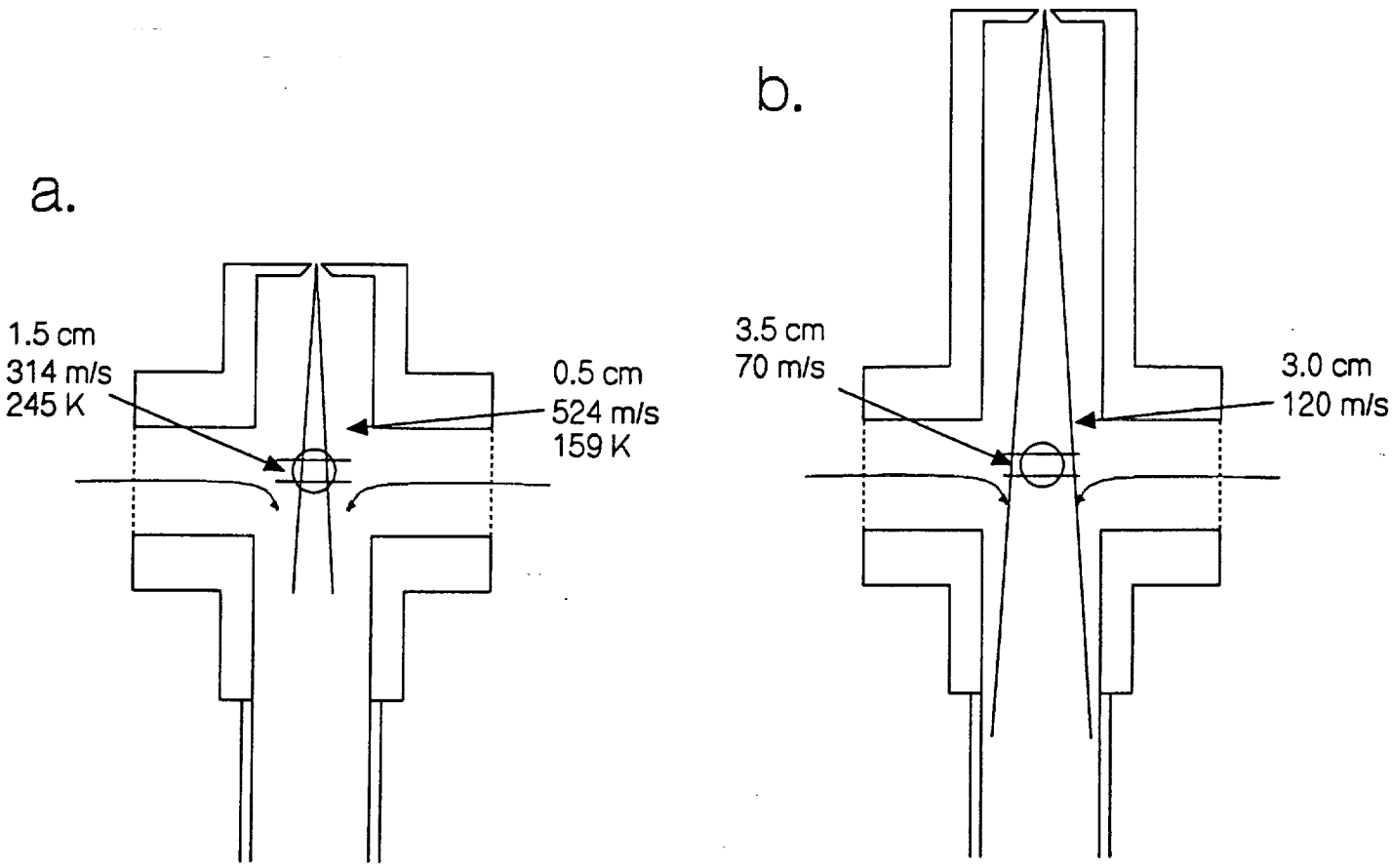

Figure 3. Schematic of the internal flow measured using a pitot tube for (a) the 9-91 prototype version, and (b) the 3-92 version. Temperatures are calculated from the velocity measurements. Notice the overlap with the laser beam (two horozontal lines) and the detector field-of-view (circle). Small flows of nitrogen or argon are added near the the White cell mirrors help confine the airstream.

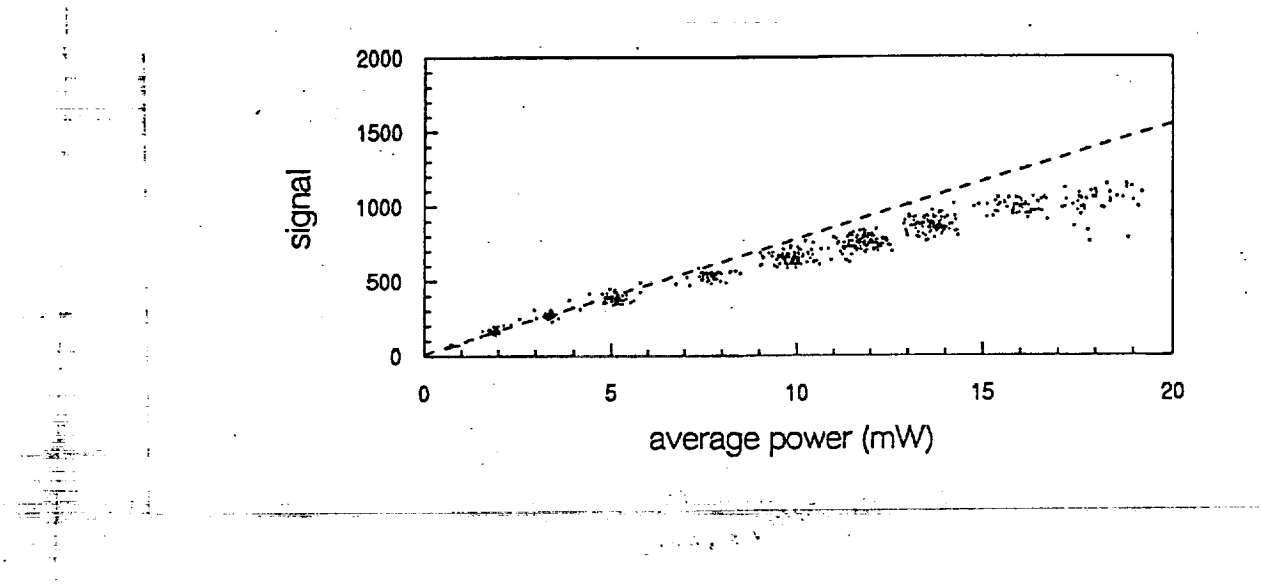

Figure 4. The measured OH signal plotted as a function of the average laser power in the White cell. The dashed line is a fit to the data when the laser power was less than 4 mW. Deviation of the measured signal from this fit shows the effect of saturation of the OH transition.

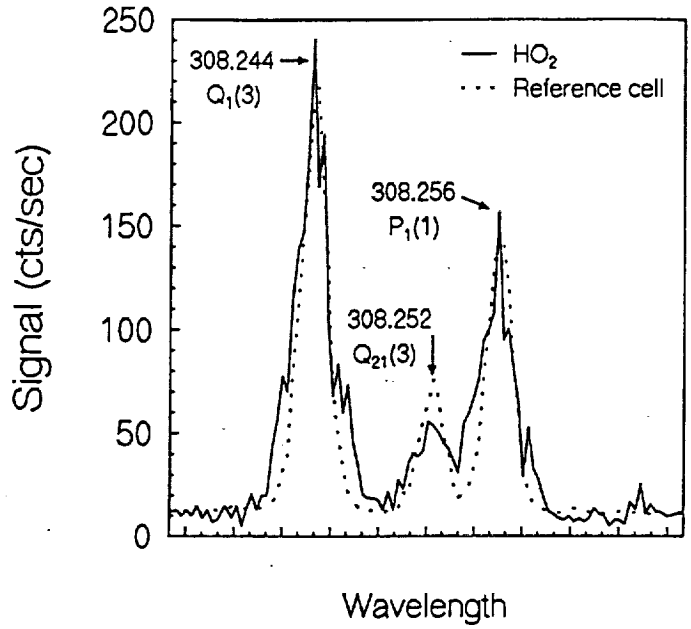

Figure 5. Spectrum of OH from partially converted ambient HO_2, recorded on March 18, 1992. The dotted line is the reference cell signal from thermal OH production. The relative peak intensities reflect changes in ambient HO_2 over the time of the scan.

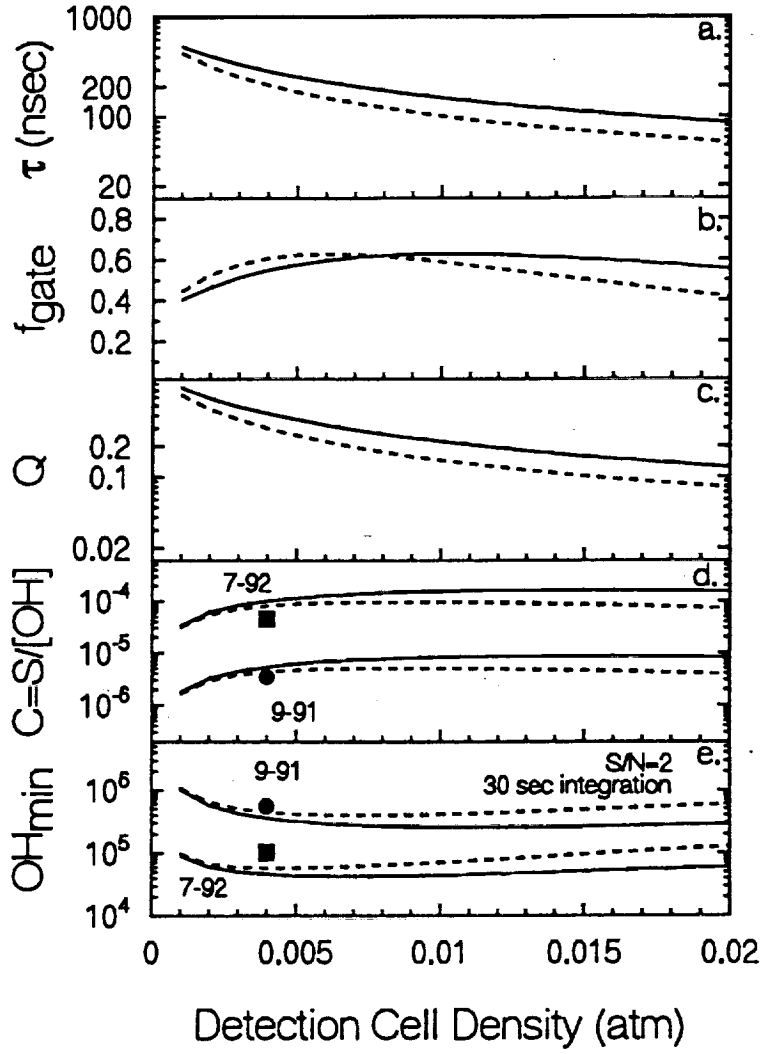

Figure 6. The effect of the total density in the detection chamber on (a) the OH lifetime; (b) the fraction of the fluorescence collected by the gated detector; (c) the quenching of the OH excited state; (d) the calculated instrument sensitivity; and (e) the calculated minimum detectable OH for 15 mW of laser power. The solid lines are for dry nitrogen and the dashed lines are for nitrogen with 2% water vapor. Filled points indicate experimental values.

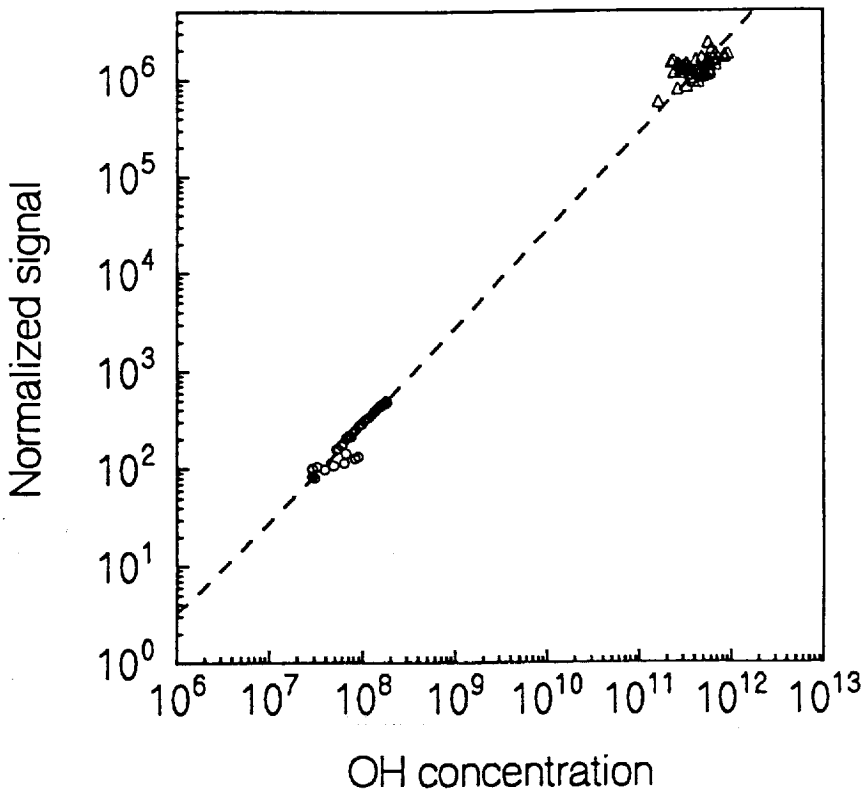

Figure 7. Log-log plot of the external OH concentration in nitrogen versus observed signal for the 7-92 prototype version. The signal is scaled to 1 mW of average laser power in the White cell. The circles are results from a calibration using the photolysis cell technique at ~15 mW average laser power. The triangles are calibration results using the absorption cell technique at average an average laser power of less than 0.005 mW.

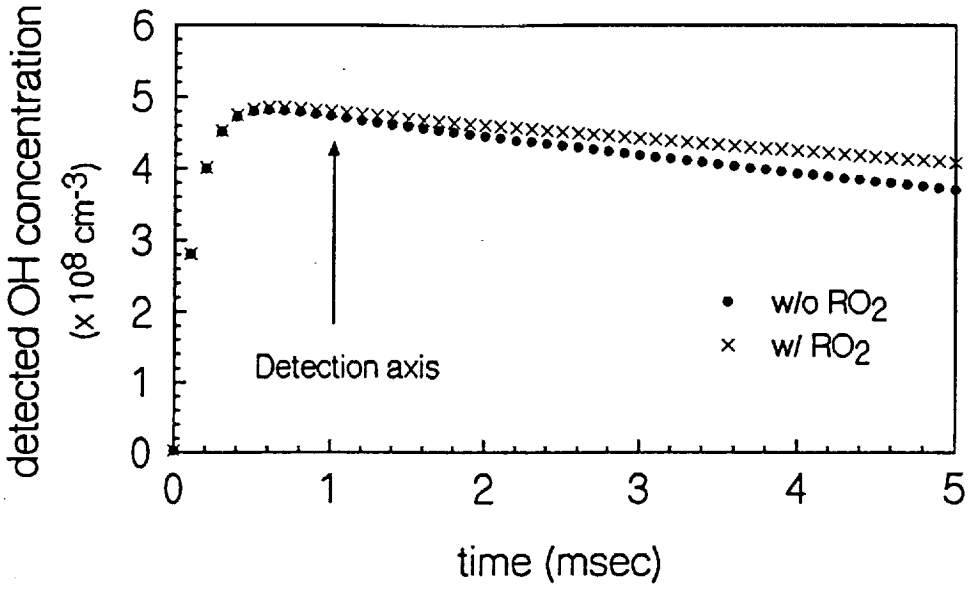

Figure 8. Simulation of the conversion of HO_2 and RO_2 to OH in the prototype instrument. The RO_2 abundance is assumed to be twice the HO_2 abundance. OH is detected approximately 1 msec after the addition point for NO.

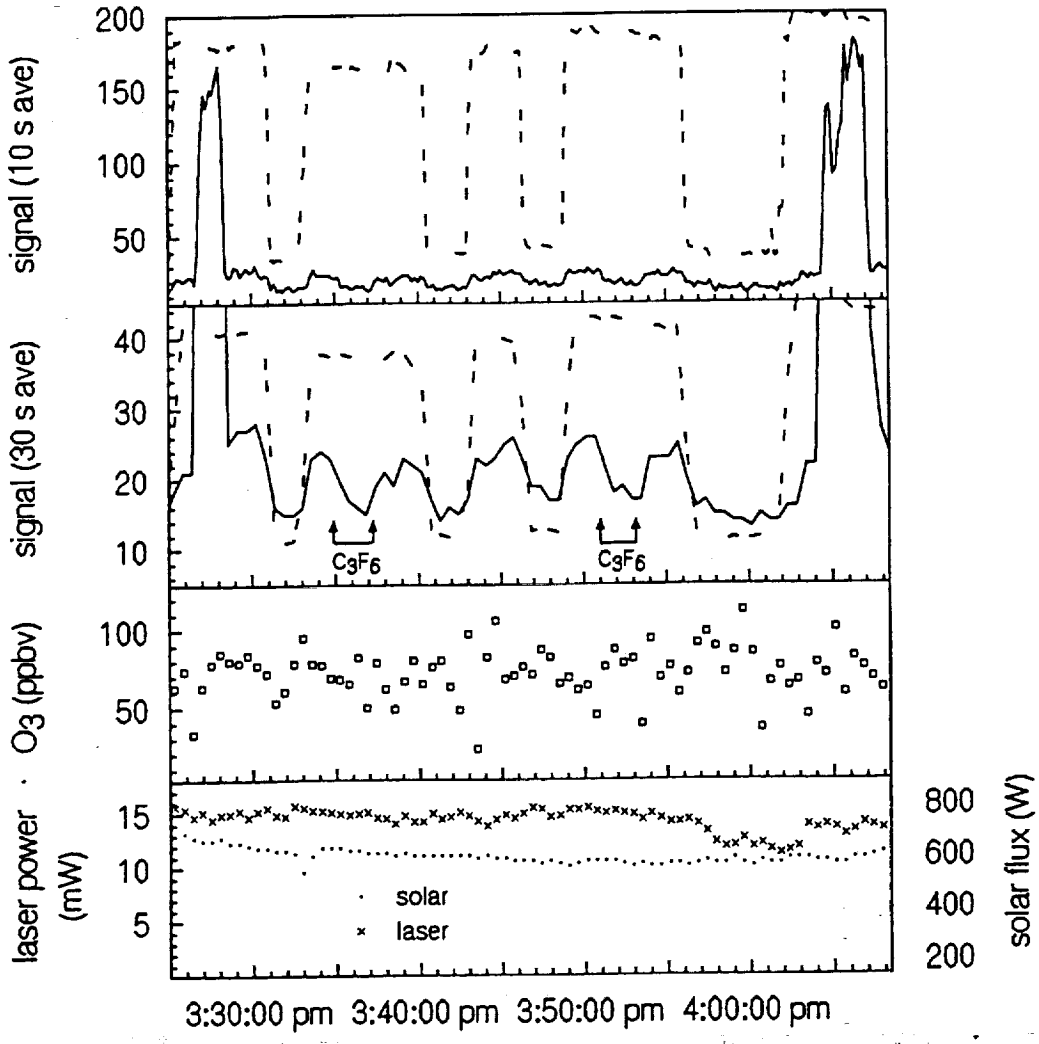

Figure 9. OH and HO_2 data from September 17, 1991, taken on the roof of the Walker Building on the Penn State campus. Shown are the OH and HO_2 signals (solid line), the reference cell signal (dashed line), O_3, laser power and solar flux. Perfluoropropylene was added at the times shown.

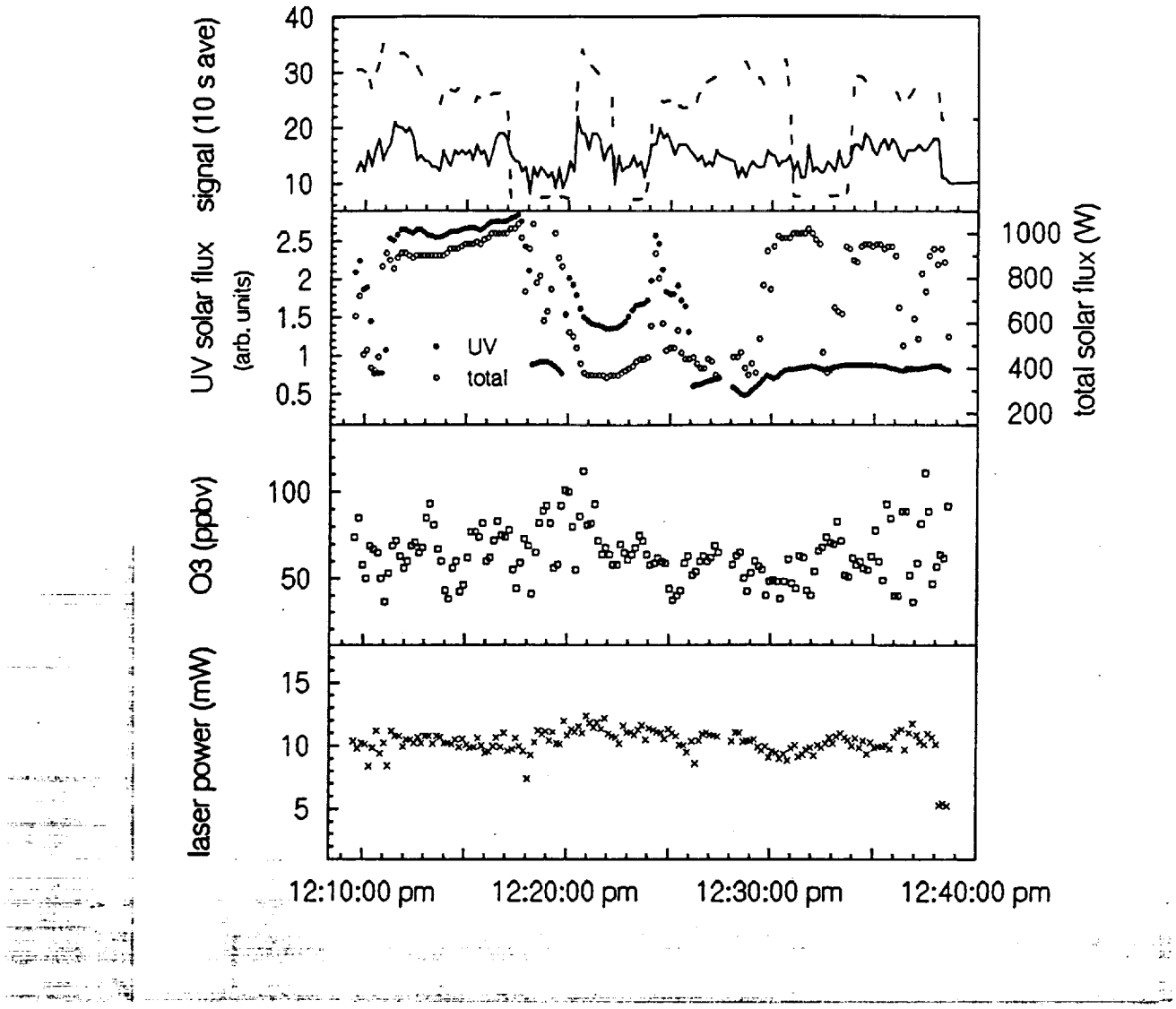

Figure 10. Sample of a 30-minute segment of data taken on September 17, 1991. Shown are the OH signal (solid line), the reference cell signal (dashed line), UV solar flux (filled circles, arbitrary units), total solar flux (open circles), O_3 and laser power. Note the correlation between the OH signal and the UV solar flux.

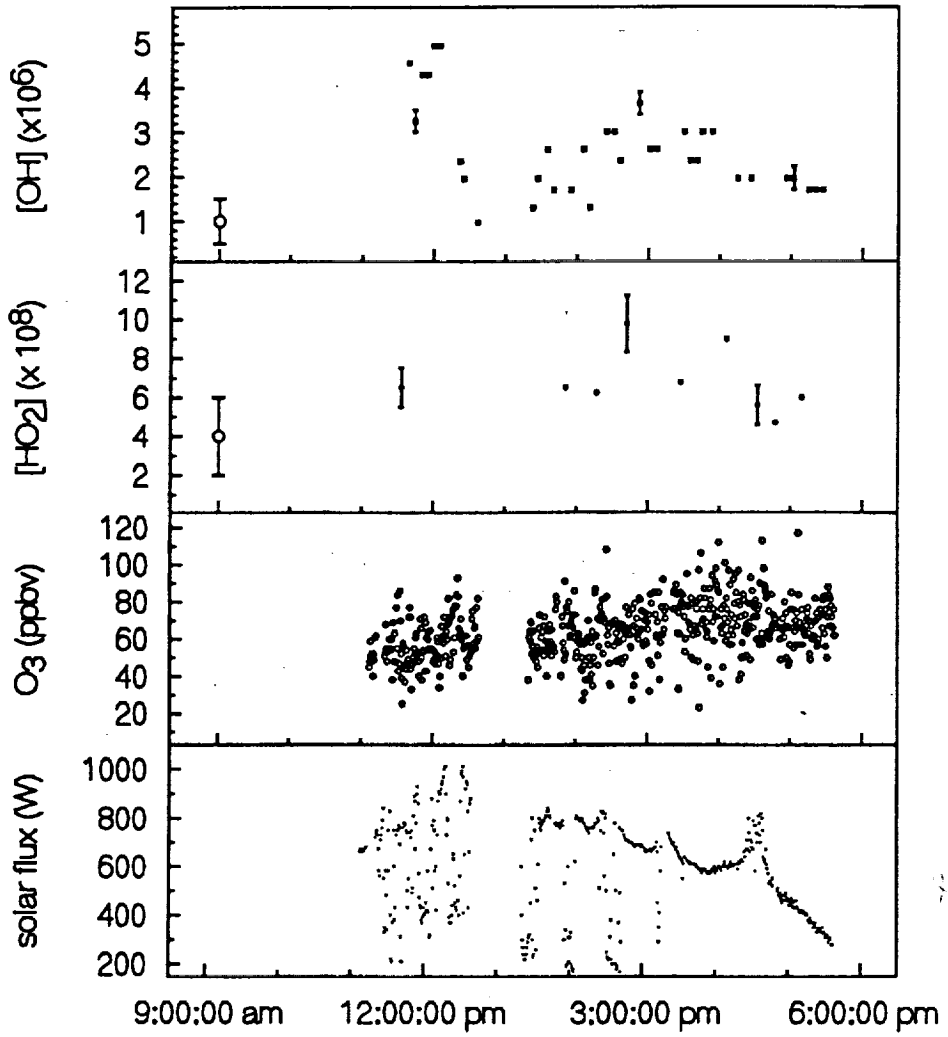

Figure 11. Measurements of OH and HO_2 as a function of time of day on September 17, 1991 from the roof of the Walker Building. Samples of the statistical errors associated with each measurement of OH and HO_2 are shown on various points. Absolute error is indicated on the left of each plot.

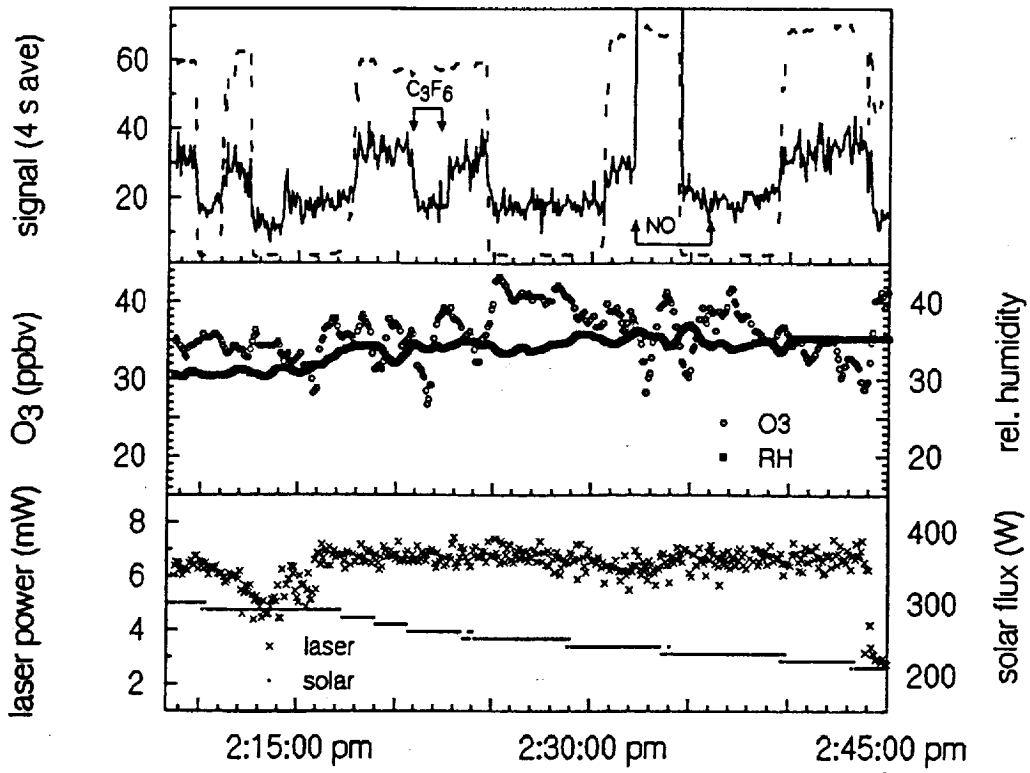

Figure 12. OH and HO_2 data from March 18, 1992 from the roof of the Walker Building. Shown are the OH signal (solid line), the reference cell signal (dashed line), O_3, relative humidity, laser power, and solar flux. C_3F_6 and NO were added at the times shown.

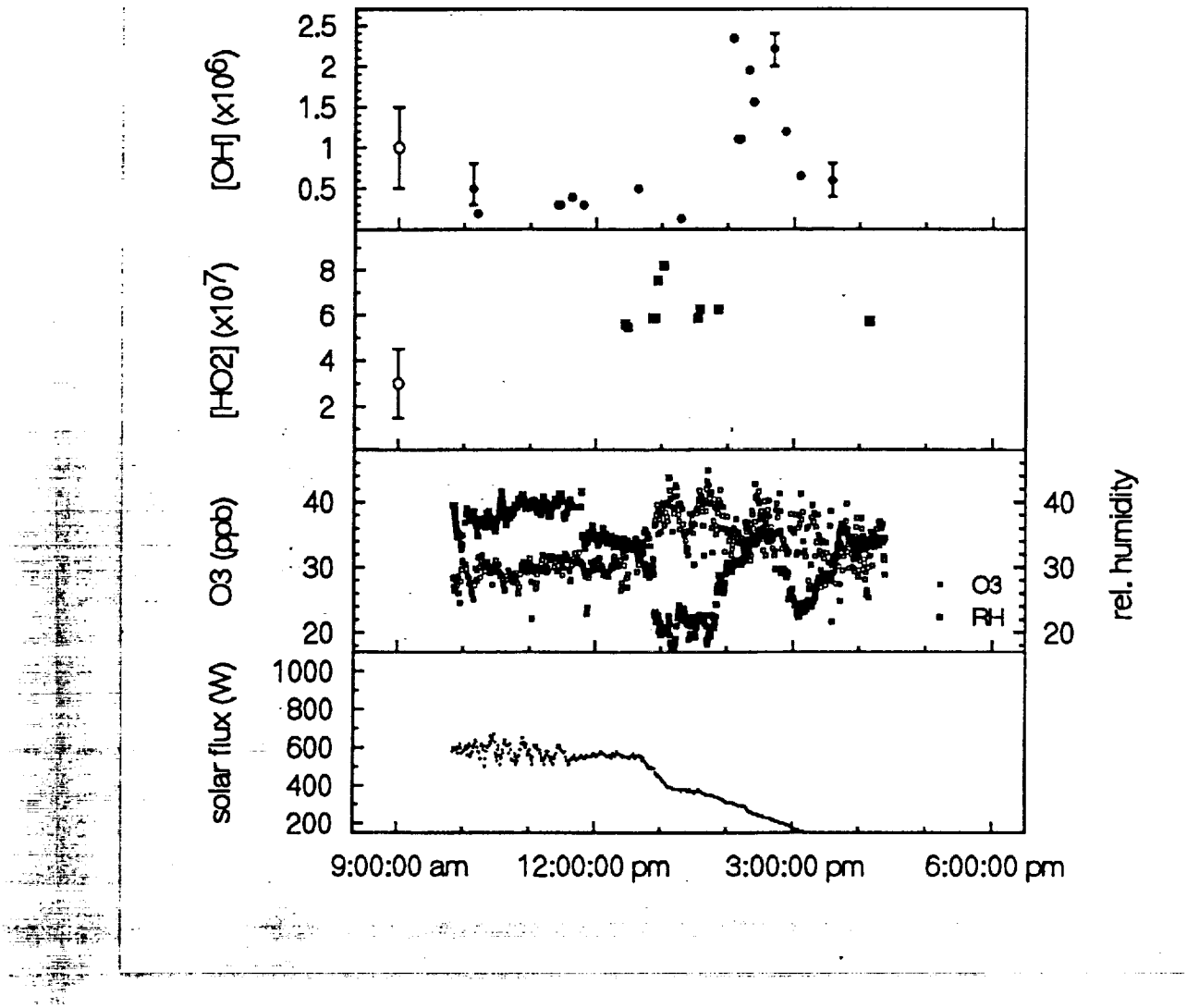

Figure 13. Measurements of OH and HO_2 as a function of time of day on March 18, 1992 from the roof of the Walker Building. Samples of the statistical errors associated with each measurement of OH are shown on various points. Statistical error for the HO_2 measurements are smaller than the points themselves. Absolute error is indicated on the left of each plot.

TABLE 1. Parameters for the OH sensitivity equation

	Prototype version		
	9-91	3-92	7-92
$B_{12}(\mathrm{cm^3\ J^{-1}\ sec^{-2}})$	1.01×10^{24}		
$\Delta\nu_D\ (\mathrm{cm^{-1}})$	0.10		
$\Delta\nu_l\ (\mathrm{cm^{-1}})$	0.15		
$\Delta N/N$	0.075		
P (W)	0.015		
l (cm)	24.0		
ϵ	0.05	0.085	
η	0.015	0.036	
T	0.05	0.075	0.23
Q	0.40		
f_{gate}	0.55		
$\rho_{\mathrm{in}}/\rho_{\mathrm{amb}}$	0.0041		
C (cts $\mathrm{sec^{-1}}/(\mathrm{OH\ cm^{-3}})$)	5.5×10^{-6}	3.3×10^{-5}	1.0×10^{-4}

TABLE 2. OH sensitivity calibration results

	Prototype version		
	9-91	3-92	7-92
Calculated (dry nitrogen)[a]	3.6×10^{-7}	2.2×10^{-6}	6.7×10^{-6}
Internal	$(2.3 \pm 0.8) \times 10^{-7}$	$(1.6 \pm 0.5) \times 10^{-6}$	
Calculated (2% water vapor)	2.8×10^{-7}	1.7×10^{-6}	5.3×10^{-6}
External		$(1.0 \pm 0.7) \times 10^{-6}$	$(3 \pm 2) \times 10^{-6}$

(*a*) sensitivities expressed in units of (counts sec^{-1} mW^{-1})/(OH cm^{-3})